Kobe University Repository : Kernel

PDF issue: 2024-08-02

Structure and Properties of Bio based Polymers

LEE SUNG LIN

(Degree)
博士（工学）

(Date of Degree)
2018-03-25

(Date of Publication)
2019-03-01

(Resource Type)
doctoral thesis

(Report Number)
甲第7195号

(URL)
https://hdl.handle.net/20.500.14094/D1007195

※ 当コンテンツは神戸大学の学術成果です。無断複製・不正使用等を禁じます。著作権法で認められている範囲内で、適切にご利用ください。

Doctoral Dissertation

博士論文

Structure and Properties of Bio based Polymers

（バイオベースポリマーの構造と物性）

January, 2018

平成 30 年 1 月

Graduate School of Engineering, Kobe University

神戸大学大学院　工学研究科

LEE SUNG LIN

李　誠潾

Table of Contents

GENERAL

INTRODUCTION

Since 1932, WH. Carothers discovered the method to synthesis Nylon [1], polymer researches have been developed dramatically. Recently, polymer materials have been used in many fields from daily usages, biomedical materials to advanced materials such as car, plane and spacecraft. This is because many polymer show not only low density and cost, but also good processability, compared with other materials such as metals or ceramics.

Recently, environmental pollution and global warming are biggest issues. In European Union, there are legislated the strict regulations about environmental problems and these restrictions are expected to be stricter. Among them, oil is regarded as the main cause of environmental problems because of oil depletion and nondegradability. Therefore, many researches are on the direction of suppressing the use of oil. There are two point of view for solving these problems. One is where it comes from (origin) and the other is where it goes (disposal). Oil is limited as a resource and more energy is required for the disposal of waste because of nondegradability. Both points of view, oil based polymers make more

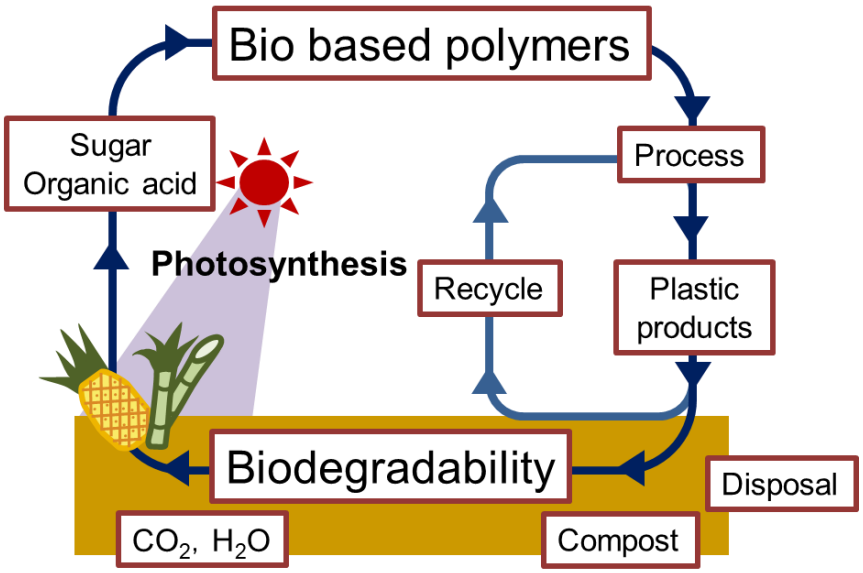

Fig. 1. Schematic of recycling biodegradable bio based polymers.

serious environmental problems. Here, bio based polymers could be one of alternative oil based polymers. Bio based polymers is synthesized by biomass, and these biomass materials are derived from tree, grain, and grass, by fermenting sugars or organic acids. Bio based polymers are paid attention materials as eco-friendly without exhaustion. In addition, after using bio based polymers, especially with biodegradability, there could be recycled directly or disposed and be composted again, as shown in Figure 1. Then, there will be tree, grain and grass again by photosynthesis. Therefore, bio based polymer materials could be permanent recyclable, and will be good for both origin and disposal way to conserve the energy.

Among biodegradable bio based polymers, poly(glycolic acid)(PGA, -$(CH_2COO)_m$-, Figure 2) possesses the simplest chemical structure of all aliphatic polyesters [2-9]. PGA is derived from glycolide obtained by the fermentation of pineapples or sugar cane. PGA show biocompatibility, biodegradability, hydrolyzability, and high mechanical properties. In addition, PGA show extremely high melting point (223 ℃) than other aliphatic polyesters, such as polycaprolactone (60℃, PCL) or polybutylene adipate (54℃, PBA). In addition, in the point of crystal structure, PGA is reported to possess planar zigzag

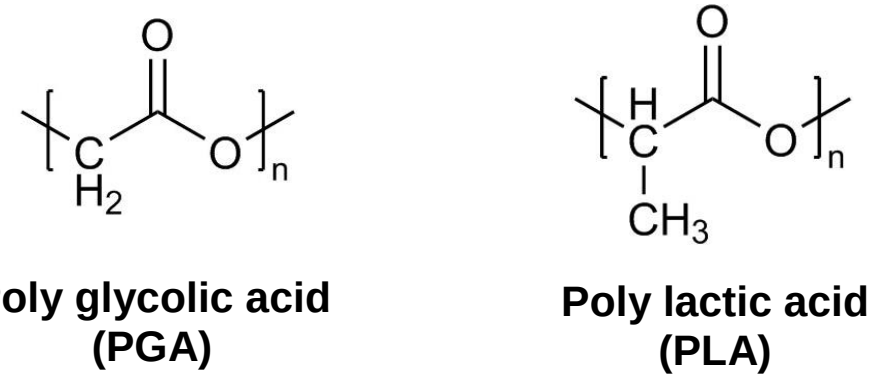

Fig. 2. Chemical structure of poly (glycolc acid) (PGA) and poly (lactic acid) (PLA).

conformation in the crystalline regions similar to polyethylene (PE) [9]. This extended planar zigzag conformation could explain the reason of higher mechanical properties of PGA than other bio based polymers. In fact, PGA has been difficult to mass-produce, so it was used only limited fields such as biomedical applications, e.g., sutures, drug delivery systems or bone fixation [5-8]. However, the KUREHA CO., has recently succeeded in mass-producing PGA. Therefore PGA is now expected to be used in a wider range of industrial fields [5]. For example, PGA is used as a temporary gauge for drilling shale gas (natural gas taken from the shale layer), because PGA possess the enough strength for endure the shale layer and biodegradability. PGA is also used as an antifouling material for marine organisms.

One of another bio based polymers, poly(lactic acid)(PLA, -$(CH_2CH(CH_3)COO)_n$-, Figure 2) is the most popular biodegradable aliphatic polyester. PLA is synthesized by ring-opening polymerization of lactide, which is obtained by fermentation of corn starch or sugar cane [10-12]. PLA also possesses biocompatibility, hydrolyzability, and low emission of greenhouse gases. Therefore, PLA is very popular material for using not only in industrial fields, but also in biomedical applications, e.g., sutures and drug delivery systems [13-18]. In addition, in 1987, Ikada *et al.* discovered same amount of blend of poly(L-lactic acid) (PLLA) and poly(D-lactic acid) (PDLA) crystallized as stereocomplex [19]. Since then, many procedures for making stereocomplex PLA (scPLA) from PLLA and PDLA were reported, such as by solution blend, in a solid state blend from the melt, during polymerizations [20-21]. scPLA is known to show different structure and properties from PLLA and PDLA. For example, scPLA shows higher melting point (~230 ℃) than those (~180 ℃) of PLLA and PDLA. The unit cell of PLLA and PDLA belongs to pseudo orthorhombic crystal system, which changes into triclinic system when

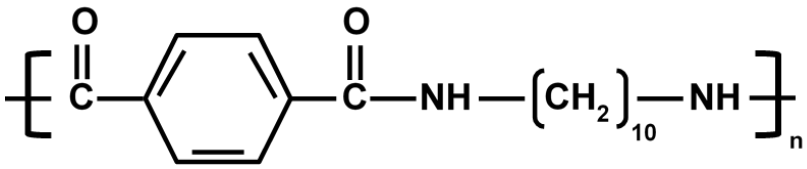

Poly(decamethylene terephthalamide) (PA10T)

Fig. 3. Chemical structure of poly(decamethylene terephthalamide) (PA10T).

stereocomplexation occurs. PLLA and PDLA are reported to possess 10_3 helical conformation in the crystal lattice. On the contrary, scPLA possesses 3_1 helical conformation, similar to isotactic polypropylene (*it*.PP) [22].

Poly(decamethylene terephthalamide) (PA10T, Figure 3) is one of another bio based polymers. PA10T is composed more than 50% of the biomass which is derived from inedible castor oil. The inedible fat oil is expected to be one of next generation resource for the bio based polymer. Due to possess high melting temperature (315 ° C), high crystallinity and high glass transition temperature (~120 ° C), PA10T is expected to be used as super engineering plastics [23].

As materials, polymers have been used in various fields, because it is easy to control the properties depending on the purpose of usages. The mechanical or thermal properties, and surface or interface properties of the polymer are highly related to structure. Among the structure factors, polymer crystal regions which is partial alignment of their molecular chains in one direction are crucial factor to compose the structure. These crystalline regions contribute to the polymer properties directly. Therefore, it is most important to investigate the exact crystal structure and properties.

The polymer chains are packed as the most stable state in the crystalline regions

according to the chain axis depending on the polymer. For example, depending on the crystal constants (the length (a,b,c) and angle (α, β, γ) of crystals), there show different lattice system. Through these constants factor, it is possible to investigate the exact lattice system, and suggest the exact crystal structure. There are lots of different lattice system, for example, orthorhombic ($a \neq b \neq c$, $\alpha = \beta = \gamma = 90°$), monoclinic ($a \neq b \neq c$, $\alpha = \gamma = 90°$, $\beta \neq 90°$) and triclinic ($a \neq b \neq c$, $\alpha \neq \beta \neq \gamma \neq 90°$) and so on.

In this thesis, it is employed the concept of the elastic modulus of the crystalline regions (crystal modulus). Crystal modulus is one of the most important mechanical properties of polymers. The crystal modulus in the directions parallel (E_l) and perpendicular (E_t) to the molecular chain axis have been measured by X-ray diffraction [24-29]. The E_l value gives the information about the skeletal conformation, deformation mechanism, and maximum modulus for the specimen modulus of polymers. The E_l values for polymers which is fully extended planar zigzag conformation in the crystalline regions are 235 GPa for PE and 250 GPa for poly(vinyl alcohol) (PVA), respectively. In contrast, the E_l value of isotactic polypropylene (*it*.PP) shows 33 GPa, which possesses helical structure in the crystalline regions. This low E_l value of *it*.PP is due to that helical skeleton is easy to elongate to the stress direction compared with the planar zigzag one. Generally, three mechanisms contribute to the molecular deformation: ① bond stretching, ② bond angle bending, and ③ internal rotating around a single bond. The ratio of force contents is 100: 10: 1 for ① bond stretching, ② bond angle bending, and ③ internal rotating, respectively. In the case of a planar zigzag skeleton of polymers, the mechanisms of bond stretching and bond angle bending contribute to the chain extension, which is the reason for the high E_l values of PE and PVA. On the other hand, the E_t values are correlated with the

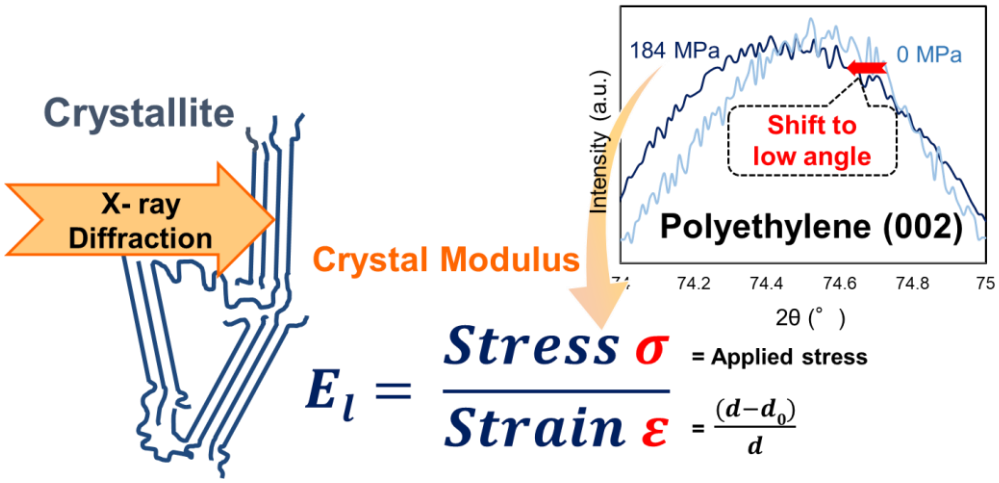

Fig. 4. The measurement of crystal modulus.

intermolecular interactions and anisotropies induced by van der Waals force, dipole-dipole interaction, and hydrogen bonding.

The crystal modulus has been measured by X-ray diffraction method. The strains in the crystalline regions is estimated by the changes in lattice spacing induced by the constant stress applied. From the interplanar distances under and after released stress, lattice strain was obtained (Figure 4). When using X-ray diffraction method, the crystalline state such as crystallite size, crystallinity are known not to effect the crystal modulus, because X-ray diffraction could detect only specific reflection of crystallite. The crystal modulus is determined as the elastic modulus when polymers are assumed to be 100 % of crystallinitiy. This is one of the advantage point of using X-ray. In this thesis, crystallite size, crystallinity, orientation of polymers are characterized. However, these are only as polymer properties, which were prove to be no influence on the crystal modulus.

Polymers are required to show high mechanical properties at very low temperature in order to be used in the nuclear and aerospace industries. The crystal modulus at cryogenic temperature gives the information about the skeletal conformation and deformation

mechanisms purely based on the elastic energy of polymer crystal, excluding the thermal effect. Nishino groups reported the E_l values of various polymers from low to high temperatures to discuss the thermal molecular motion in the crystalline regions. The investigations of the E_l values for atactic PVA [28] and nylon-6 [29] revealed significantly depend on temperature, which is affected by incoherent thermal molecular motions in the crystalline regions.

Moreover, for extending the application fields of polymer, Nanoscale fibers (nanofibers) were investigated recently. In a past few decades, nanoscale materials are the subject of extensive worldwide researches. Because of their novel functionality and high performance, nanoscale materials were discussed not only in academia but also many different types of applications are attempted within the textile, aerospace industry and so on. Nanofibers show high specific surface area and low structural defects. Electrospinning (ES) is well known as a low cost but effective method to produce polymer nanofibers [30-31]. It is a unique approach using electrostatic forces to produce fibers from polymer solutions or molten polymers, and the spun nanofibers possess a smaller diameter and larger surface area than those obtained from conventional spinning process. Thus, ES became well-recognized method and has already created interesting applications in drug delivery system, wound dressing, scaffolds in tissue engineering, and sensors in electronics [32-33]. In general, ES is used to make nonwoven fabric. However, this thesis employed one distinguished different point. Instead of using flat plate collector, it is used a rotating drum collector, which make fibers well-aligned. Then, aligned nanofibers could be uniaxially drawn under heating to promote crystallization and uniaxial molecular orientation, which is expected to result in higher mechanical properties.

In this thesis, the crystal modulus of bio based polymer PGA and PLA were evaluated by X-ray diffraction, and the skeletal conformation, deformation mechanism, maximum modulus, intermolecular interaction and anisotropy with temperature dependence were investigated. Based on the information on the maximum modulus of PGA, PGA nanofibers were prepared and compared the properties in order to achieve the maximum modulus. In fact, the crystal modulus of PLLA were reported by many papers, but those of PDLA, scPLA, especially about PGA, are not reported yet. In addition, for PA10T, the crystal lattice constant is needed to measure the crystal modulus. Therefore, crystal lattice constant was determined first, then the crystal modulus was investigated. Concerning these contents, this thesis was divided into four chapters, and explaining in detail as following:

Chapter I is concerned the crystal modulus E_l and E_t of PGA by X-ray diffraction. And it is investigated the ralationships among the mechanical properites in the crystalline regions. The skeletal conformation is formed to be contracted conformation in the crystalline regions, and the intermolecular interaction is higher than other polymers with temperature dependence for PGA. In addition, the reason of high melting point of PGA is explained from mechanical point of view.

Chapter II is concerned the highly oriented PGA nanofibers by electrospinning collected on a rotating drum in order to make fibers well-aligned. Well-aligned nanofibers were also possible to make uniaxial orientation of molecular chain by uniaxial drawing and annealing. Then, PGA nanofibers are expected to show high mechanical properteis and approaching to maximum modulus. Therefore, the structure and properties of the well-aligned and well-oriented PGA nanofibers were evaluated.

Chapter III is concerned the crystal modulus E_l and E_t of PLLA, PDLA, and scPLA by X-ray diffraction. It is investigated the difference of crystal modulus of PLLA, PDLA and scPLA by mechanical point of view. Then, scPLA was shown to possess different strucutre and properties from PLLA and PDLA, as higher melting point and higher mechanical properteis. In addition, the skeletal structure, intermolecuar cohesive energy of PLLA, PDLA and scPLA were discussd. As a result, the intermolecular interaction of scPLA was higher than those of PLLA and PDLA, even PLAs and scPLA possess van der Waals intermolecular interaction. In this chapter, the reason of higher melting point of scPLA was explained from mechanical point of view.

Chapter IV is concerned with structure and properties of PA10T. PA10T crystal lattice was investigated by X-ray diffraction method, for the meridional and equatorial directions. Then, using the information of obtained crystal lattice, crystal modulus E_l were investigated. In addition, not only crystal properties, but also bulk properties and surface properties were reported in this thesis.

References

(1) Carothers, W. H.; Bickford, C. F.; Hurwitz, G. J. *J. Am. Chem. Soc.* **1927**, *49* (11), 2908–2914

(2) Carothers, W. H.; Dorough, G. L.; Natta, F. J. *J. Am. Chem. Soc.* **1932**, *54* (2), 761–772

(3) Kister, G.; Cassanas, G.; Vert, M. *Spectrochim. Acta - Part A Mol. Biomol. Spectrosc.* **1997**, *53* (9), 1399–1403

(4) Sekine, S.; Yamauchi, K.; Aoki, A.; Asakura, T. *Polymer* **2009**, *50* (25), 6083–6090

(5) Yamane, K.; Sato, H.; Ichikawa, Y.; Sunagawa, K.; Shigaki, Y. *Polym. J.* **2014**, *46* (11), 769–775

(6) Gilding, D. K.; Reed, A. M. *Polymer* **1979**, *20* (12), 1459–1464

(7) Zong, X. H.; Wang, Z. G.; Hsiao, B. S.; Chu, B.; Zhou, J. J.; Jamiolkowski, D. D.; Muse, E.; Dormier, E. *Macromolecules* **1999**, *32* (24), 8107–8114

(8) Lee, J. W.; Gardella, J. A. *Macromolecules* **2001**, *34* (12), 3928–3937

(9) Chatani, Y.; Suehiro, K.; Ô kita, Y.; Tadokoro, H.; Chujo, K. *Die Makromol. Chemie* **1968**, *113* (1), 215–229

(10) Tsuji, H. Hydrolytic Degradation. In *Poly(Lactic Acid)*; Auras, R., Lim, L.-T., Selke, S. E. M., Tsuji, H., Eds.; John Wiley & Sons, Inc.: Hoboken, NJ, USA, 2010; pp 343–381.

(11) Ikada, Y.; Tsuji, H. *Macromol. Rapid Commun.* **2000**, *21* (3), 117–132

(12) Tsuji, H.; Ikada, Y. *Polymer* **1995**, *36* (14), 2709–2716

(13) Tsuji, H.; Noda, S.; Kimura, T.; Sobue, T.; Arakawa, Y. *Sci. Rep.* **2017**, *7*, 45170

(14) Penning, J. P.; Dijkstra, H.; Pennings, A. J. *Polymer* **1993**, *34* (5), 942–951

(15) Gogolewski, S.; Pennings, A. J. *J. Appl. Polym. Sci.* **1983**, *28* (3), 1045–1061

(16) Leenslag, J. W.; Gogolewski, S.; Pennings, A. J. *J. Appl. Polym. Sci.* **1984**, *29* (9), 2829–2842

(17) Athanasiou, K. A.; Niederauer, G. G.; Agrawal, C. M. *Biomaterials* **1996**, *17* (2), 93–102

(18) Hoffman, A. S. *Adv. Drug Deliv. Rev.* **2012**, *64*, 18–23

(19) Ikada, Y.; Jamshidi, K.; Tsuji, H.; Hyon, S. H. *Macromolecules* **1987**, *20* (4), 904–906

(20) Tsuji, H. *Macromol. Biosci.* **2005**, *5* (7), 569–597

(21) Tsuji, H. *Adv. Drug Deliv. Rev.* **2016**, *107*, 97–135

(22) Okihara, T.; Tsuji, M.; Kawaguchi, A.; Katayama, I.; Tsuji, H.; Hyon, S.; Ikada, Y. *J. Macromol. Sci. Part B Phys.* **1991**, *30:1-2*, 119–140

(23) Liu, H.; Yang, G.; He, A.; Wu, M. *J. Appl. Polym. Sci.* **2004**, *94* (2), 819–826

(24) Nakamae, K.; Nishino, T.; Shimizu, Y.; Matsumoto, T. *Polym. J.***1987**, *5*, 451–459.

(25) Nishino, T.; Matsui, R.; Nakamae, K. *J. Polym. Sci. Part B Polym. Phys.* **1999**, *37* (11), 1191–1196

(26) Nishino, T.; Miki, N.; Mitsuoka, Y.; Nakamae, K.; Saito, T.; Kikuchi, T. *J. Polym. Sci. Part B Polym. Phys.* **1999**, *37* (23), 3294–3301

(27) Nishino, T.; Tada, K.; Nakamae, K. *Polymer* **1992**, *33* (4), 736–743.

(28) Nakamae, K.; Nishino, T.; Ohkubo, H.; Matsuzawa, S.; Yamaura, K. *Polymer* **1992**, *33* (12), 2581–2586

(29) Nakamae, K.; Nishino, T.; Hata, K.; Matsumoto, T. *KOBUNSHI RONBUNSHU* **1987**, *44* (6), 421–428

(30) Bhardwaj, N.; Kundu, S. C. *Biotechnol. Adv.* **2010**, *28* (3), 325–347

(31) Huang, Z. M.; Zhang, Y. Z.; Kotaki, M.; Ramakrishna, S. *Compos. Sci. Technol.* **2003**, *63* (15), 2223–2253

(32) Kakade, M. V.; Givens, S.; Gardner, K.; Lee, K. H.; Chase, D. B.; Rabolt, J. F. *J. Am. Chem. Soc.* **2007**, *129* (10),

(33) Tsuji, H.; Nakano, M.; Hashimoto, M.; Takashima, K.; Katsura, S.; Mizuno, A. *Biomacromolecules* **2006**, *7* (12), 3316–3320

CHAPTER I

Elastic Modulus of the Crystalline Regions of Poly (Glycolic Acid)

1.1 Introduction

Poly(glycolic acid)(PGA, -(CH2COO)$_m$-) is the simplest aliphatic polyesters as one of bio based polymer [1-9]. PGA is derived from glycolide fermented by pineapples or sugar cane. PGA show biocompatibility, biodegradability, hydrolyzability, and high mechanical properties. Noteworthy, PGA possesses extremely high melting point (223 ℃) than other aliphatic polyesters, such polycaprolactone (60℃) or polybutylene adipate (54℃). PGA has been difficult to mass-produce, so it was used only limited fields. However, the KUREHA CO., has recently succeeded in mass-producing PGA, so PGA is now expected to be used wide industrial fields [10].

PGA is reported to possess planar zigzag conformation in the crystalline regions, and similar structure of polyethylene (PE) [9]. This extended planar zigzag conformation could explain why PGA possess high mechanical properties compare with other bio based polymers.

The crystal modulus is one of most important mechanical properties of polymers. The crystal modulus in the directions parallel (E_l) and perpendicular (E_t) to the chain axis have been measured using X-ray diffractions [11-16]. These crystal modulus gives us information about not only the skeletal conformation, deformation mechanism, maximum modulus, but also intermolecular interactions such as van der Waals, hydrogen bonding, and dipole-dipole interactions together with their anisotropies. Also, the crystal modulus at cryogenic temperature gives us information about the skeletal conformation and deformation mechanisms purely based on polymer crystal, excluding the thermal effect.

In this chapter, using X-ray diffraction method, measured the E_l and E_t values of PGA, and then investigated the relationships among the mechanical properties in the crystalline

regions, the skeletal conformation of molecular chains, and the intermolecular interactions. In addition, the melting point is defined as the change in melting entropy (ΔS) and melting enthalpy (ΔH), $\Delta H/\Delta S$. The E_l and E_t values can correlate with ΔS and ΔH, respectively. It is possible to expect to use the E_l and E_t values to reveal the reason for the high melting point of PGA from a mechanical point of view. Furthermore, temperature dependence of the crystal modulus was also investigated to examine the thermal properties of the crystalline regions of PGA.

1.2. Experimental

1.2.1. Sample Preparation

PGA pellets were kindly supplied KUREHA CO., (KUREDUX B35®). PGA pellets were hot-pressed at 523 K, following by quenching in ice water. A PGA film (film thick : 26 μm) was uniaxially drawn 4 or 6 times its original length (20 mm) at 323 K. Then, drawn film was annealed at 383 K or 453 K for 10 min at a constant length. PGA film is generally hard to draw due to its fast crystallization, but by rapid drawing just after quenching, it was succeeded at attaining a high draw ratio, prior to crystallization starting.

1.2.2. Characterization

The densities d of the drawn and annealed PGA films were measured by a floatation method, using benzene and carbon tetrachloride system at 303 K.

The mechanical properties of drawn and annealed PGA films (2 mm wide and 20 mm long) were measured at an extension rate of 2 mm/min using an Autograph AGS-1kND

tensile tester (Shimadzu) at 300 K. The cross-section was prepared by cutting the film and the cross-sectional area was evaluated from the density, weight, and length of the sample. The means and standard deviations were calculated for the macroscopic specimen modulus (Y_l), tensile strength (σ_{max}), and elongation at break (ε_{max}) measured minimum five samples.

The melting point (T_m) and ΔH of PGA were measured using a differential scanning calorimeter (Rigaku Co., DSC 8230) with a sample weight of 5 mg, with heating rate of 5 ℃/min. T_m and ΔH were determined as the peak temperature and area of the whole melting endotherm, respectively. PGA crystallinity X_c was evaluated with the following equation (1.1).

$$X_c = \Delta H / \Delta H_0 \tag{1.1}$$

where ΔH_0 = 135 J/g for 100 % crystallinity [17].

The PGA dynamic viscoelastic properties (20 mm long) were measured using a dynamic mechanical analyzer (DVA-220S, ITK Ltd.) at a heating rate of 6 K/min and a frequency of 10 Hz. A tensile deformation of 0.25 % was applied to the sample. Also, the temperature of the most intense relaxation peak on the tan δ versus temperature curve was defined as the glass transition temperature T_g.

X-ray diffraction photographs were recorded on an imaging plate, a camera length of 72 mm. The specimen was irradiated perpendicular to the fiber axis with the Cu$K\alpha$ radiation generated by a Rigaku RINT-2000 for 30 min, operating at 40 kV and 20 mA.

To obtain the crystallite size D_{hkl}, the observed profiles for the (*hkl*) planes were corrected for the instrumental broadening according to the following equation (1.2).

$$\beta^2 = B^2 - b^2 \quad (1.2)$$

where β is the pure integral width of the reflection, B and b are the integral widths of the reflection for the drawn and annealed PGA films and a standard sample (0.89), respectively. The correction for the doublet, Cu$K\alpha 1$ and Cu$K\alpha 2$, broadening was calculated by the Jones method [18]. Finally, D_{hkl} were calculated using the Scherrer equation (1.3).

$$D_{hkl} = \lambda / \beta \cos \theta \quad (1.3)$$

where θ is the Bragg angle of the reflections, and λ is the X-ray wavelength (1.54Å).

The degree of the crystallite orientation π was defined by the equation (1.4)

$$\pi = (180 - H^\circ)/180 \quad (1.4)$$

where H° is the half-width of the intensity distribution curve for the equatorial 110 reflection of PGA along the Debye-Scherrer ring.

1.2.3. Elastic Modulus of the Crystalline Regions

The lattice extension under a constant load was measured by means of an X-ray diffractiometer equipped with a stretching device and a load cell. (Figure 1.1 show X-ray diffraction profiles for the (002) plane of PGA not loading, 380 MPa loading and after unloading at 300 K, for example.) The strain ε in the crystalline regions was estimated using the equation (1.5):

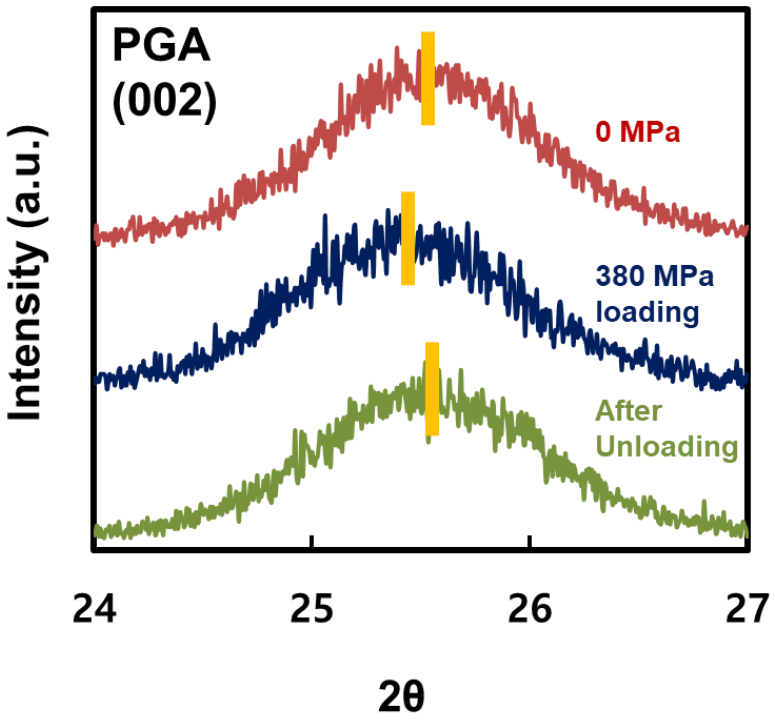

Fig. 1.1 X-ray diffraction profiles for the (002) plane of PGA not loading, 380 MPa loading and after unloading at 300K.

$$\varepsilon = \Delta d / d_0 \tag{1.5}$$

where d_0 denotes the initial lattice spacing, and Δd is the change in lattice spacing induced by a constant stress. The experimental error in measuring the peak shift was evaluated ordinarily to be less than ±0.01 ° at a 2θ angle.

The stress σ in the crystalline regions was assumed to be equal to the stress applied to the sample. This assumption of a homogeneous stress distribution has been proven experimentally for PE and cellulose [19-20].

The crystal modulus E_l and E_t were calculated by the equation (1.6)

$$E_{l,t} = \sigma_{l,t} / \varepsilon_{l,t} \tag{1.6}$$

where subscripts $_l$ and $_t$ mean the direction parallel and perpendicular to the chain axis ,

respectively.

The measurements have been described in more detail in Nishino Laboratory publications [11-16, 19-23].

Crystal modulus measurements at cryogenic temperature were performed with a cryogenic cell (Iwatani Industrial Gases Corp. Ministat CRT-006-7000, Figure 1.2) constructed in Nishino laboratory [23]. In these measurements, a stretching device and a load cell were combined with a cryostat cell and mounted on an X-ray goniometer. Helium gas was compressed and transported into the cold head attached to the top of the cryostat cell. Then, helium was adiabatically expanded, so the cold head was cooled to a cryogenic temperature of 13 K. The samples were clamped to the stretching device under a vacuum and cooled by thermal conduction via the clamp connected to the cold head. Full details are described elsewhere [21-23].

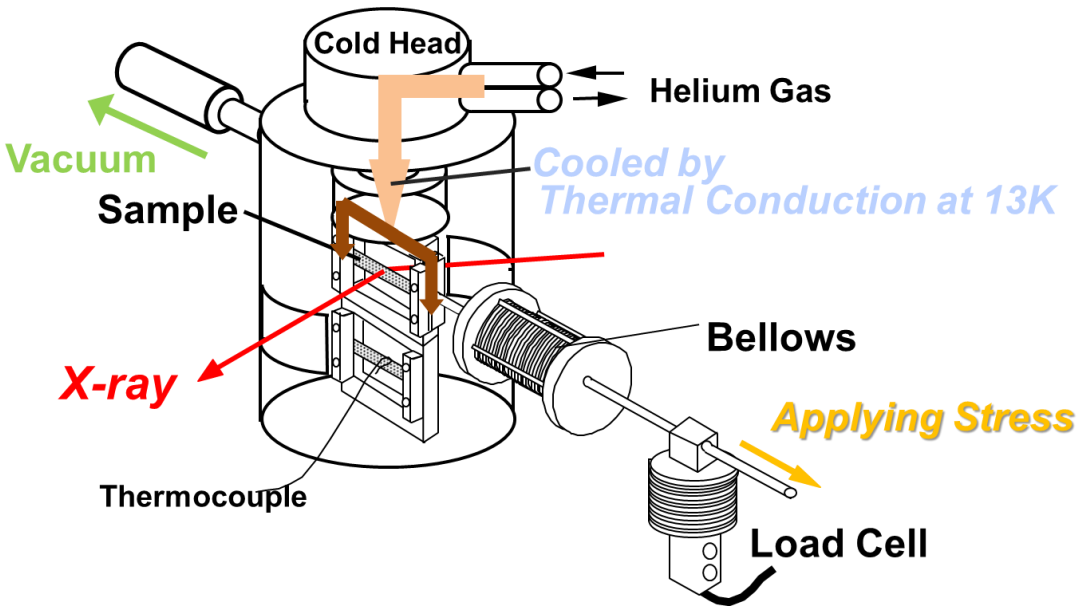

Fig. 1.2 Schematic diagram of X-ray diffraction apparatus with a stretching device for the measurement of crystal modulus at cryogenic temperature.

1.3. Results and Discussion

1.3.1. Sample Characteristics

Figure 1.3 shows X-ray fiber photograph of drawn (6 times) and annealed PGA film at 300 K. PGA crystallites were highly oriented along the drawn direction and highly crystallized.

Figure 1.4 shows equatorial and meridional X-ray diffraction profiles of drawn (6 times) and annealed PGA film at 300 K. On the basis of the reported crystal lattice of PGA (orthorhombic, a = 5.22 Å , b = 6.19 Å , c (fiber axis) = 7.02 Å) [9], the diffraction peaks was indexed as shown in the figure. Meridional 002 and 006 reflections were used to measure the E_l values, equatorial 110 and 020 reflections were used to measure the E_t values, respectively. Drawn and annealed PGA films in this study were more highly oriented and highly crystallized than the sample reports by Oca *et al.*[17].

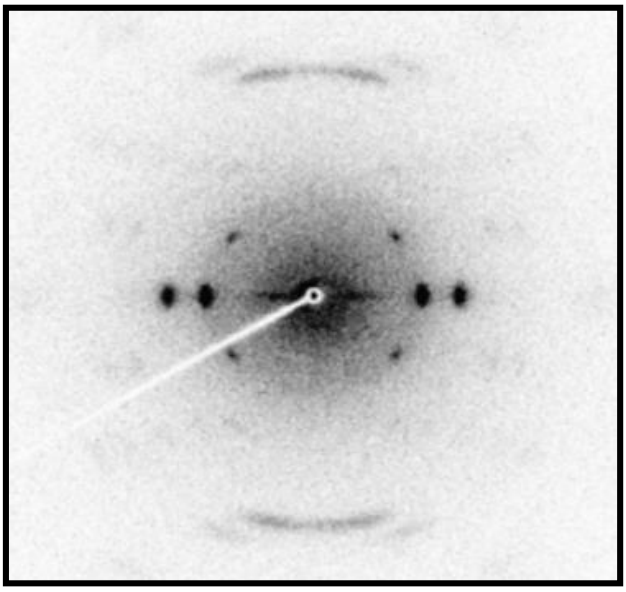

Fig. 1.3 X-ray fiber photograph of drawn (6 times) and annealed PGA film at 300 K.

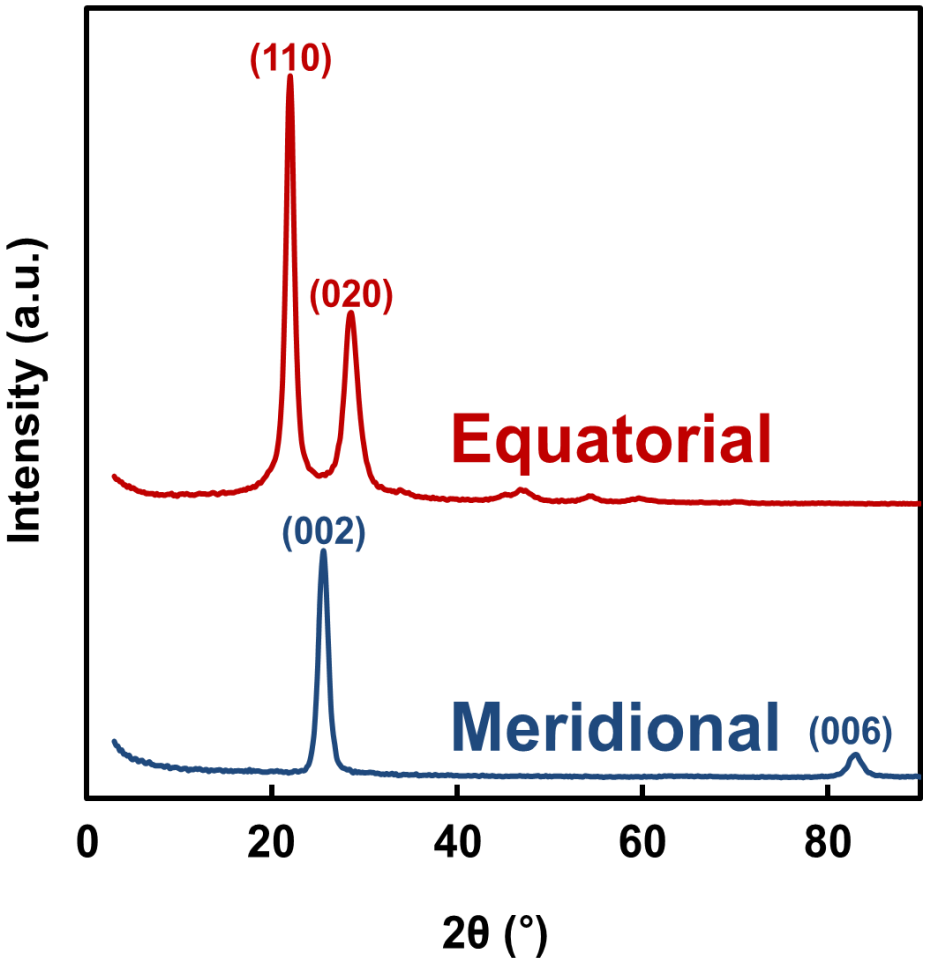

Fig. 1.4 Equatorial and meridional X-ray diffraction profiles of drawn (6 times) and annealed PGA film at 300 K.

Table 1.1 shows crystallite orientation, crystallinity, crystallite size, melting point T_m, Young's modulus Y_l, tensile strength σ_{max} and elongation at the break ε_{max} of drawn and annealed PGA films. Annealing process was prepared at 110 ℃ for 10 min. The drawn (6 times) and annealed PGA films showed a high degree of the crystallite orientation and high crystallinity. The crystallite size for the 006 reflection, melting temperature and Y_l value increased as draw ratio increased. It is noteworthy that a microstructural change of only a few percent caused to double for the Y_l value.

Table 1.1 Crystallite orientation, crystallinity, crystallite size, melting point T_m, Young's modulus Y_l, tensile strength σ_{max} and elongation at the break ε_{max} of drawn and annealed PGA. Annealing was prepared at 110 °C, 10 min.

PGA	λ = 4 @50 °C	λ = 6 @50 °C
Crystallite orientation	0.950	0.955
Crystallinity (%)	62.7	69.7
Crystallite size (Å)		
(002)	80	178
(006)	54	74
(110)	119	122
(020)	45	45
T_m (°C)	221	223
Y_l (GPa)	10	20
σ_{max} (MPa)	294	548
ε_{max} (%)	18	12

1.3.2. Crystal Modulus E_l

Figure 1.5 shows the stress-strain curves of various conditions drawn and annealed PGA films at 300 K. All the plots could be expressed with a straight line with the same inclination through the origin, and the lattice extensions were always reversible. The inclination of this line gave the crystal modulus E_l, and the E_l value of PGA show 104 GPa at 300 K.

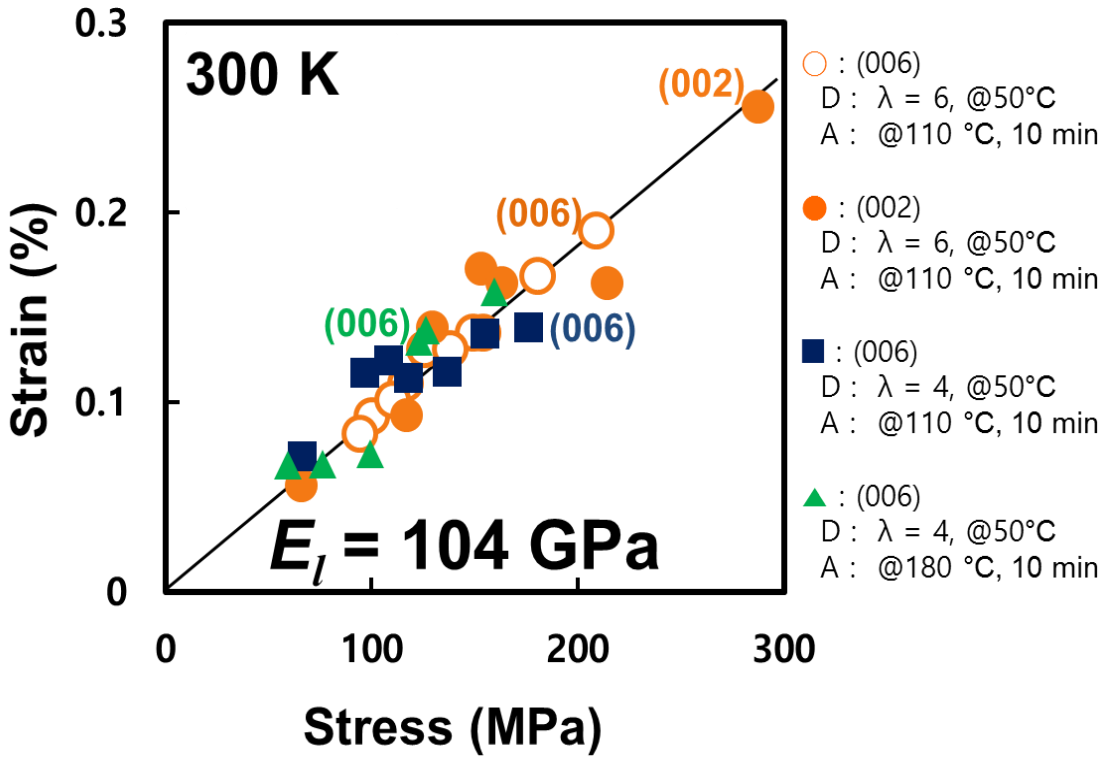

Fig. 1.5 Stress-strain curves of various conditions drawn and annealed PGA films at 300 K.

The E_l value (104 GPa) of PGA resembles that (108 GPa) of poly(ethylene terephthalate) (PET), however, it is much lower than that (235 GPa) of PE as a fully extended planar zigzag conformation in the crystalline regions [19]. If the PGA skeleton is fully extended planar zigzag conformation as reported, the E_l value of PGA should be as same as that of PE. In fact, when the E_l value by Treloar's method [24-25] for the fully extended planar zigzag skeleton of PGA by using reported bond lengths, bond angles and these force constants, the calculated value was 237 GPa, which is almost equal to that of PE.

This study use both 002 and 006 reflections for the lattice strain measurements, when Oca *et al.* [17] reported the crystal modulus of 77 GPa for PGA using only the 002 reflection. When using X-ray diffraction method, the 0.01° error in 2θ measurements corresponds to 0.0387 % for the 002 reflection and 0.009 % for the 006 reflection,

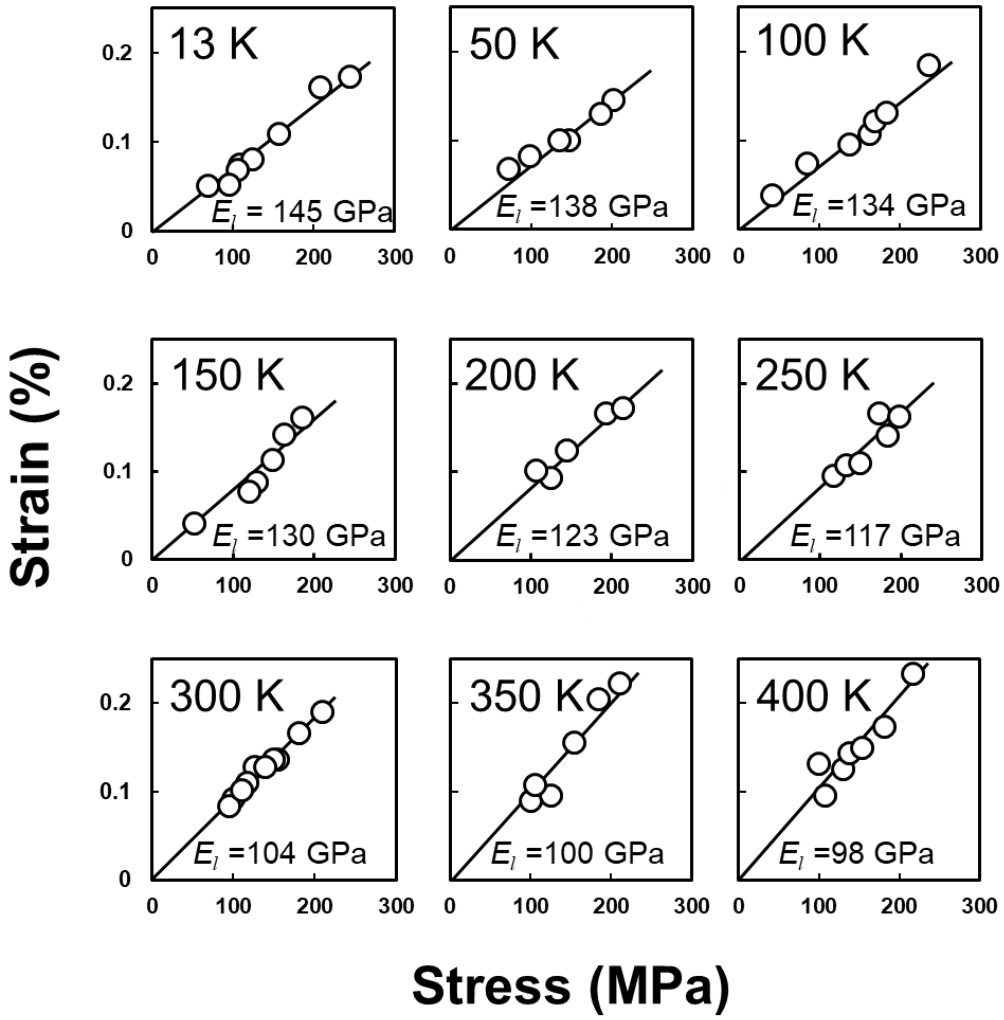

Fig. 1.6 Stress-strain curves for the (006) plane of PGA at various temperature.

respectively, thus this study show higher reliability. Oca *et al.* also calculated the E_l value of 294 GPa for planar zigzag conformation, but that a low observed E_l value of PGA is attributed by inhomogeneous stress distribution. However, as surely shown in Figure 1.5, the same crystal modulus E_l for PGA with different microstructures supports the homogeneous stress distribution.

Figure 1.6 shows stress-strain curves for the (006) plane of PGA at various temperature. From the initial inclination, E_l value was calculated and shown in figure, respectively. At

13 K, the E_l value was 145 GPa, indicating a 40 % increment above that 104 GPa at room temperature. The inclinations of stress-strain curves are risen up gradually, when temperature increasing. And higher temperatures, the E_l values decreased and reach to 98 GPa at 400 K. PGA show temperature dependence for E_l value.

Figure 1.7 shows the temperature dependence of the crystal modulus E_l, and chain contraction from planar zigzag for the (006) plane of PGA, together with a mechanical tan δ of drawn and annealed PGA film. PGA show temperature dependence for crystal modulus and contraction of the fiber period. From figure, the temperature dependence of the E_l values show similar trend of the contraction of the fiber period. Even at 13 K, the

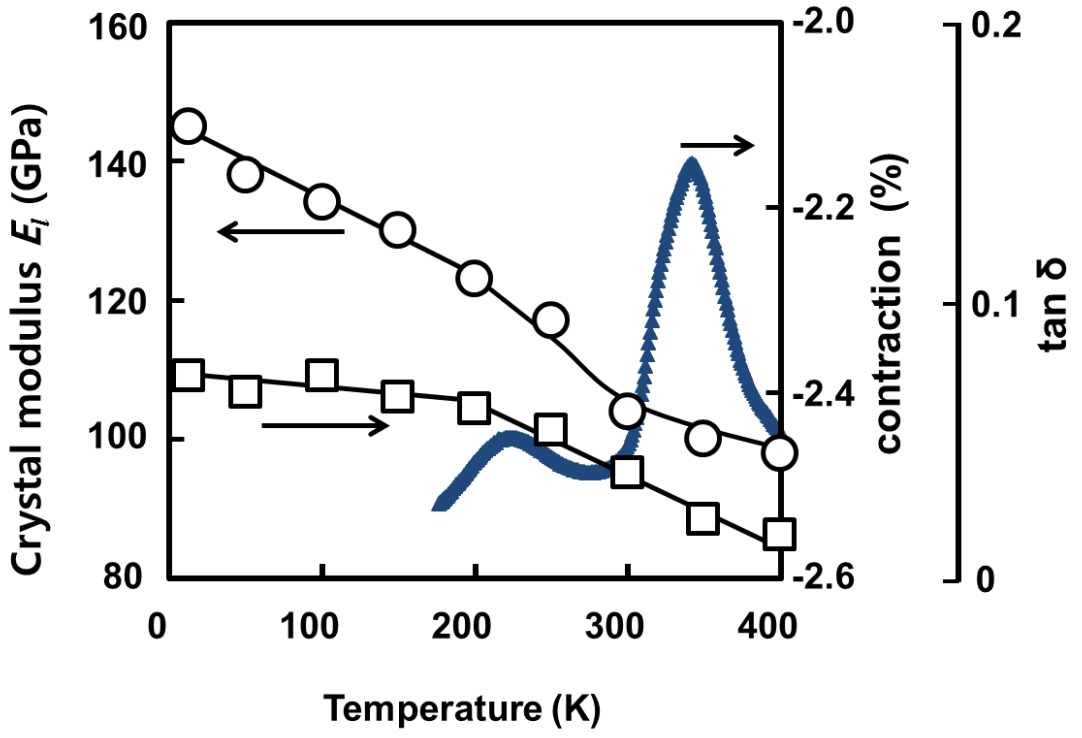

Fig. 1.7 Temperature dependence of (○) the crystal modulus E_l, (□) chain contraction from planar zigzag for the (006) plane and (◆) mechanical tanδ of drawn and annealed PGA film.

PGA chain did not reach a fully extended state but contracted approximately 2.4 %. This suggests the PGA skeleton is intrinsically contracted in the crystalline regions, through the internal rotation. It could be clearly manifested by the E_l measurement, though this contraction might be negligibly small when evaluated from X-ray fiber patterns. Oca *et al.* [26] also suggested the skeleton of PGA is contracted from planar zigzag conformation by nuclear magnetic resonance (NMR) measurements, which supports this results.

The abrupt change of both the E_l values and chain contraction of PGA were observed around 200 K. Being accompanied with these changes, mechanical tan δ changed around 200 K, which suggests the molecular motion in the crystalline regions of PGA was activated around 200 K. In general, the molecular motion of a polymer is referred as *α, β, γ* relaxation from high to low temperatures. In figure 1.7, the tan δ peak around 330 K could be said *α* relaxation, in other word, the glass transition temperature of PGA (approximately 50 ℃ measured by DSC). Then, the tan δ peak around 200 K would be *β* relaxation.

In order to compare the rigidity of a chain skeleton itself while eliminating the cross-sectional area effect, here use the *f*-value, the force required to stretch a molecule by 1 %, calculated from the E_l value and the cross-sectional area (16.15 $Å^2$) of one molecule in a crystal lattice.

Figure 1.8 shows the relationship between the contraction from planar zigzag molecular conformation and the *f*-values of polyesters and poly(*α*-olefin)s. Table 1.2 shows the E_l values and *f*-values of PGA, PET, and PE at 13 K and 300 K, for comparison. As the chain contraction increases, the *f*-value decreases for both polyesters and poly(α-olefin)s. In addition, this trend is manifested much more for polyesters than poly(α-olefin)s. This is

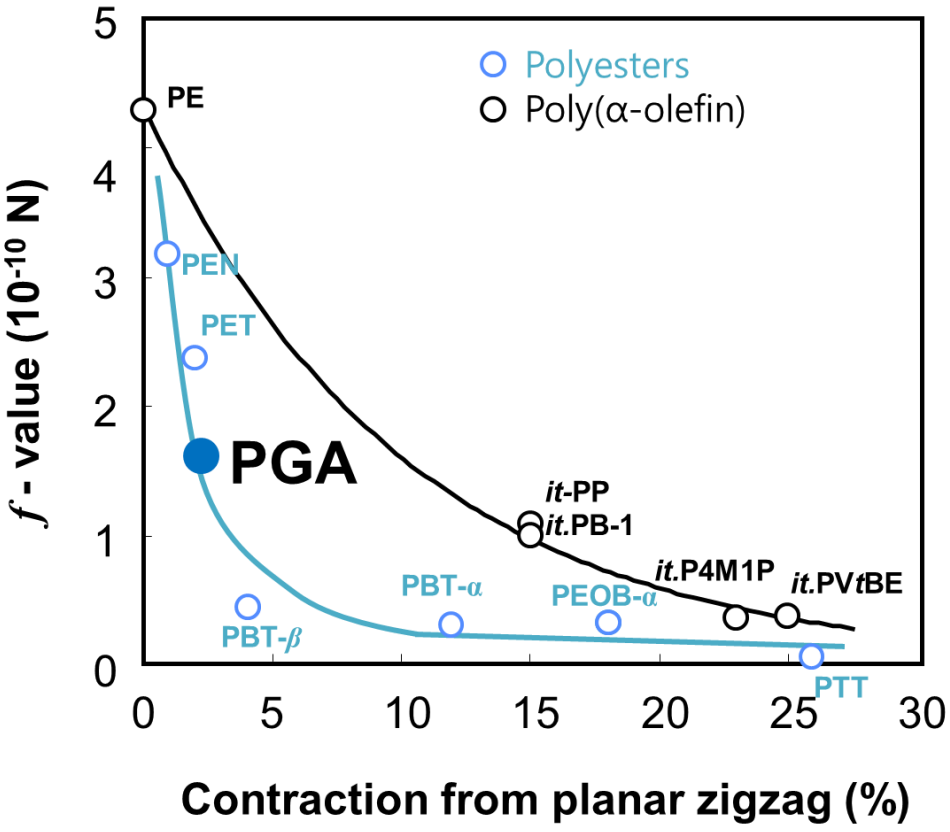

Fig. 1.8 Relationships between contraction from planar zigzag molecular conformation and the *f*-value of polyesters, and poly(α-olefin)s.

due to the force constant for the deformation of ester groups (C-O-C) being smaller than that of carbon-carbon linkages (C-C-C).

The observed *f*-value of PGA is 1.68 x 10^{-10} N, and fit into the line for polyesters, which is much smaller than that (4.28 x 10^{-10} N) of PE and even smaller than that (2.20 x 10^{-10} N) of PET. PGA shows a smaller *f*-value due to a smaller cross-sectional area than PET (20.40 $Å^2$), although PET and PGA show similar E_l values at 300 K.

Accordingly, as mentioned above, PGA skeleton is not fully extended but possesses contracted conformation in the crystal lattice. It need to figure out the chain contraction by kinked chain model of PGA, as like PE [19] and ethylene-vinyl alcohol copolymer

Table 1.2 The E_l values and *f*-values of PGA, PET, PE at 13 K and 300 K.

	E_l		*f*-value	
	GPa		10^{-10} N	
	13 K	300 K	13 K	300 K
PGA	145	104	2.34	1.68
PET	108	108	2.20	2.20
PE	235	235	4.28	4.28

(EVA) [27]. For PE and EVA, their chain contraction were very small (around -0.1 % to -0.6 %), from the fully extended zigzag conformation. In these cases, drastic changes of the E_l value could be explained using kinked chain model, where small amount of defect largely influenced the E_l value. However, PGA skeleton has already largely contracted (-2.4 %) even at cryogenic temperature. Then the thermal contraction changed up to -2.6 % at 400 K. In the case of PGA, kinked chain model effect is not enough to explain the changes of the chain contraction and temperature dependence of the E_l value simultaneously. Therefore, we considered that the kinked chain model is not suitable for PGA.

In addition, the low E_l value is considered to cause small melting entropy ΔS, which contributes to the increase of T_m of PGA.

1.3.3. Crystal Modulus E_t

Figure 1.9 show the stress σ - strain ε curves for the equatorial orange (110) and blue (020) planes of PGA at (open circles) 300 K and (filled circles) 13 K, respectively. The curves for the reflections could be expressed with a straight line through the origin, and the lattice extensions were always reversible. The E_t values of PGA were 7.3 and 5.8 GPa for the (110) and (020) planes at room temperature, respectively. The E_t value (7.3 GPa) for the (110) plane of PGA is noticeably higher than that (4.3 GPa) of PE only based on van der Waals intermolecular interaction, and resembles that (6.6 GPa) of PVA based on intermolecular hydrogen bonds and that (9 GPa) of polyoxymethylene (POM) based on dipolar-dipolar interaction. These results suggest PGA possess strong intermolecular interactions in the crystal lattice.

The inclination stress σ - strain ε curves in Figure 1.9 decreased as temperature decreased, which reveals the E_t value increased around 1.5 times at 13 K compared with those at

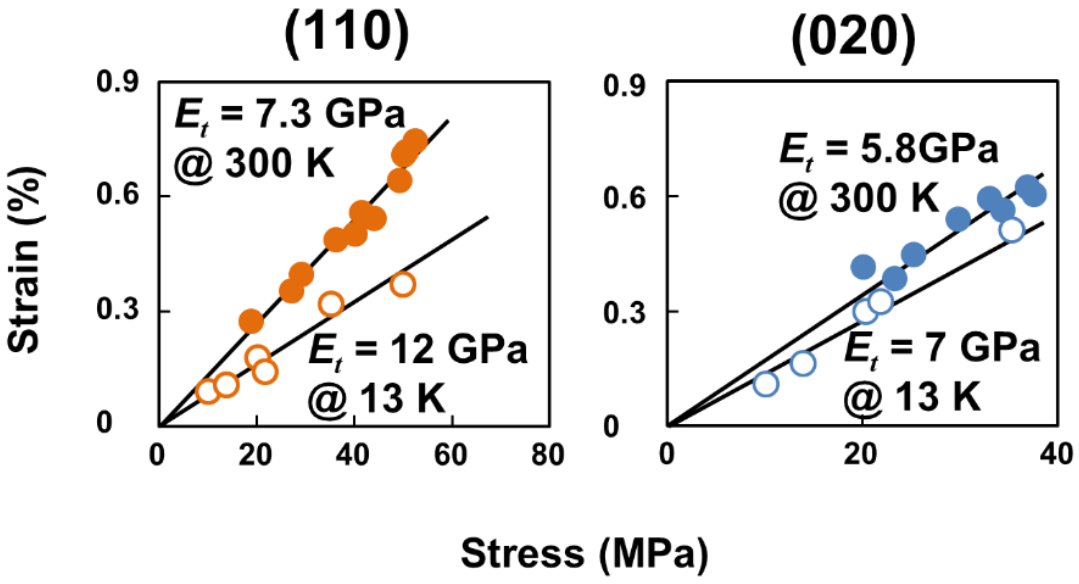

Fig. 1.9 Stress-strain curves for the (110) and (020) planes of drawn and annealed PGA film at 13 K and 300 K.

room temperature. Therefore, temperature dependence act in not only the chain direction but also the intermolecular direction in the crystalline regions of PGA.

Figure 1.10 shows the tem temperature dependence of the lattice spacing for the (110) and the (020) planes of PGA from 13 K to 300 K. As temperature increased, the lattice spacing for both planes expanded. These results suggest intermolecular interaction for both plane decreased as temperature increased, which is considered to result in the decrease of the E_t values. In addition, during thermal expansion, inflectional points are observed around 200 K for both planes. Across 200 K, the thermal expansion coefficient (α) changed approximately 3 times as shown in the figure. Accompanied by the crystalline dispersion in macroscopic tan δ shown in Figure 1.7, the molecular motion in the crystalline regions enhanced around 200 K, which results in the temperature dependence of both E_l and E_t of PGA.

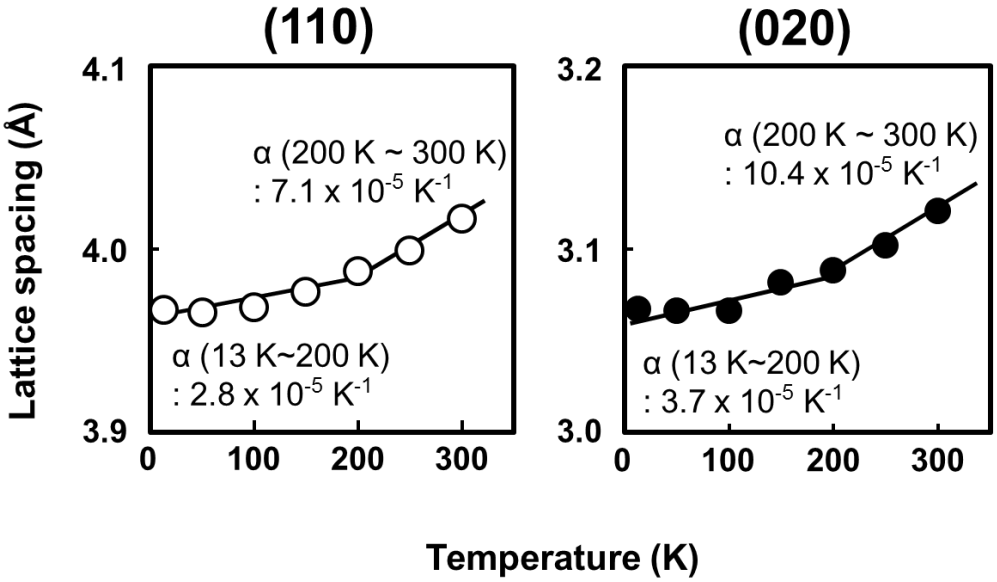

Fig. 1.10 Temperature dependence of the lattice spacing for (○) (110) and (●) (020) plane of PGA from 13 K to 300 K.

Table 1.3 summarizes the E_t values at 13 K and 300 K, melting points and thermal expansion coefficients α of PGA, PVA [15], and high density polyethylene (HDPE) [19], for comparison. The α value for the 020 reflection was higher than that for the 110 reflection at all temperatures. Sato *et al.* [28] and Pan *et al.* [29] measured the lattice parameter using 110 and 020 reflections from room temperature to high temperature. They also observed that the 020 reflection shows larger thermal expansion than the 110 reflection. These results reliably explain that the 110 reflection gave higher E_t value than the 020 reflection. In addition, they suggest that the 110 reflection possesses hydrogen bonding between the C-H…O interactions, among polymer chains in the crystalline regions, using IR spectroscopy, quantum mechanical and natural bond orbital (NBO) calculation methods.

Table 1.3 The E_t values at 13 K, 300 K, melting point T_m and thermal expansion coefficient α of PGA, PVA and HDPE.

	E_t		T_m	α
	13 K	300 K		
	GPa		°C	10^{-5} K^{-1}
PGA				
(110)	12	7.3	223	2.8 (13 K ~ 200 K) 7.1 (200 K ~ 300 K)
(020)	7	5.8		3.7 (13 K ~ 200 K) 10.4 (200 K~ 300 K)
PVA				
(200)	17	6.6	230	5.9 (200 K ~ 300 K)
HDPE				
(200)	11	3.2	135	11.8 (200 K ~ 300 K)

The cross-sectional area (16.15Å^2) of one molecule in the crystal lattice PGA is smaller than that of PE (18.24Å^2). This shows highly closed packing of PGA chains in the crystalline regions. This also contributes to high density (1.54 g/cm^3) and higher E_t value for PGA than for PE.

Figure 1.11 shows the anisotropies of the crystal modulus E_t values at 13 K and 300 K, together with those of α (13 K ~ 300 K) projected on the chain packing in the *ab* plane of the PGA crystal lattice. PGA possesses high anisotropy in the direction perpendicular to

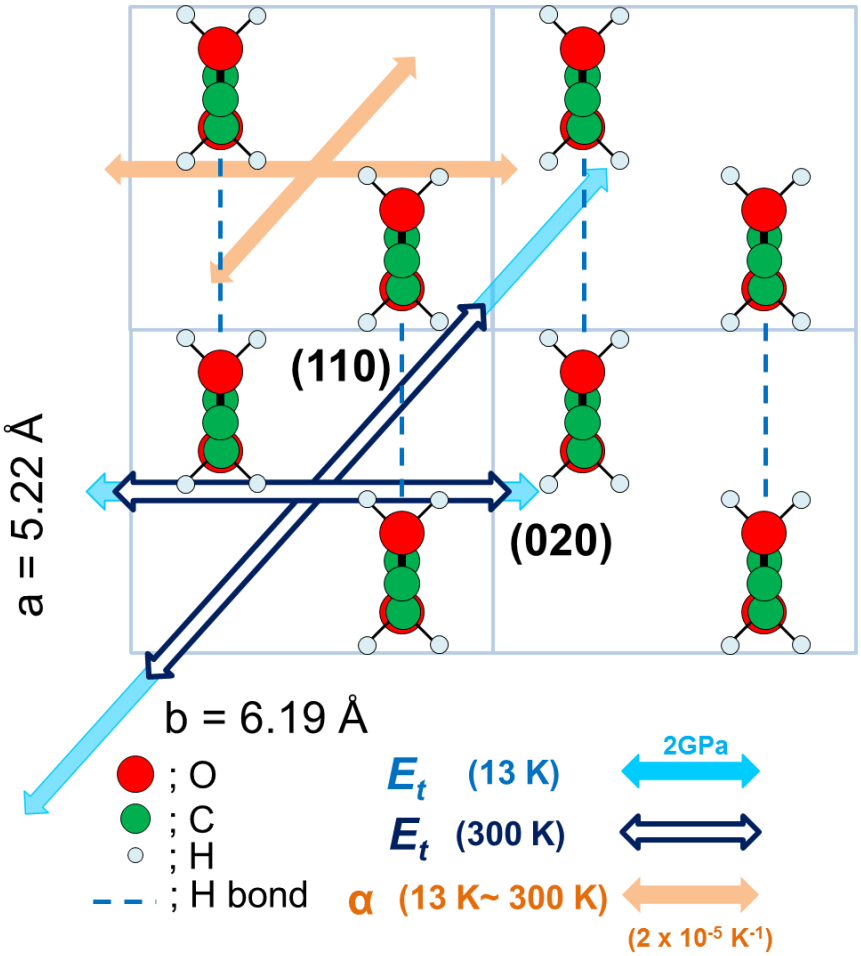

Fig. 1.11 Anisotropy of crystal modulus E_t and thermal expansion coefficient α in the *ab* plane of PGA at 13 K and 300 K.

the chain axis. The E_t value of the (110) plane was higher than that of the (020) plane as shown in the figure. In contrast, the α value of the (020) plane is larger than that of the (110) plane. These results reveal that the microscopic mechanical properties of the molecular chain correlate with thermal properties.

The E_t values of PGA were quite high, which may cause high melting enthalpy ΔH. As described above, the low E_l value is suggested to cause low entropy ΔS of PGA. Therefore, both the high E_t value (increase of enthalpy ΔH) and the low E_l value (decrease of entropy ΔS) are considered to contribute to the high melting point of PGA from a mechanical point of view.

1.4. Conclusions

Crystal modulus in the directions parallel (E_l) and perpendicular (E_t) to the chain axis of poly(glycolic aicd) (PGA) were measured by X-ray diffraction. The crystal modulus E_l shows a PGA skeleton is not fully extended but contracted from a planar zigzag one. The E_l value of PGA shows temperature dependence from cryogenic temperature to high temperature. Around 200 K, abrupt changes of both E_l values and chain contraction were considered to be caused by molecular motion in the crystalline regions. The high crystal modulus E_t suggested high intermolecular interaction acts between PGA chains. Both the low E_l value and high E_t value are considered to contribute to the high melting point of PGA.

1.5. References

(1) Carothers, W. H.; Dorough, G. L.; Natta, F. J. *J. Am. Chem. Soc.* **1932**, *54* (2), 761–772

(2) Kister, G.; Cassanas, G.; Vert, M. *Spectrochim. Acta - Part A Mol. Biomol. Spectrosc.* **1997**, *53* (9), 1399–1403

(3) Sekine, S.; Yamauchi, K.; Aoki, A.; Asakura, T. *Polymer* **2009**, *50* (25), 6083–6090

(4) Hiraoka, Y.; Kimura, Y.; Ueda, H.; Tabata. Y. *Tissue Engineering* **2003**, *9*, 1101–1112.

(5) Gilding, D. K.; Reed, A. M. *Polymer* **1979**, *20* (12), 1459–1464

(6) Zong, X. H.; Wang, Z. G.; Hsiao, B. S.; Chu, B.; Zhou, J. J.; Jamiolkowski, D. D.; Muse, E.; Dormier, E. *Macromolecules* **1999**, *32* (24), 8107–8114

(7) Lee, J. W.; Gardella, J. A. *Macromolecules* **2001**, *34* (12), 3928–3937

(8) You, Y.; Min, B.; Lee, S.; Lee, T.; Park, W. *J. Appl. Poly. Sci.* **2005**, *95*, 193-200

(9) Chatani, Y.; Suehiro, K.; Ô kita, Y.; Tadokoro, H.; Chujo, K. *Die Makromol. Chemie* **1968**, *113* (1), 215–229

(10) Yamane, K.; Sato, H.; Ichikawa, Y.; Sunagawa, K.; Shigaki, Y. *Polym. J.* **2004**, *46*, 769-775

(11) Nakamae, K.; Nishino, T.; Shimizu, Y.; Matsumoto, T. *Polym. J.* **1987**, *19*, 451-459

(12) Nishino, T.; Matsui, R.; Nakamae, K. *J. Polym. Sci., Part B: Polym. Phys.* **1999**, *37*, 1191-1196

(13) Nishino, T.; Miki, N,; Mitsuoka, Y.; Nakamae, K.; Saito, T.; Kikuchi, T. *J. Polym. Sci., Part B: Polym. Phys.* **1999**, *37*, 3294–3301

(14) Nishino, T.; Tada, K,; Nakamae, K. *Polymer* **1992**, *33*, 736-743

(15) Nakamae, K.; Nishino, T.; Ohkubo, H.; Matsuzawa, S.; Yamaura. K. *Polymer* **1992**, *33*, 2581-2586

(16) Nakamae, K.; Nishino, T.; Hata, K,; Matsumoto, T. *Kobunshi Ronbunshu* **1987**, *44*, 421-428

(17) Oca, H.; Ward, I. *Polymer* **2006**, *47*, 7070-7077

(18) Jones, F. *Proc. R. Soc. Lond. A* **1938**, *166*, 16-43

(19) Nakamae, K.; Nishino, T.; Ohkubo, H. *J. Macromol. Sci., Phys.* **1991**, *B30*, 1-23

(20) Sakurada, I.; Ito, T.; Nakamae, K, *Makromol. Chem.* **1964**, *75*, 1-10

(21) Nishino, T.; Okamoto, T.; Sakurai, H. *Macromolecules* **2011**, *44*, 2106-2111

(22) Kotera, M.; Nakai, A.; Saito, M.; Izu, T.; Nishino, T. *Polym. J.* **2007**, *39*, 1295-1299

(23) Nishino, T.; Miyazaki, H.; Nakamae, K. *Rev. Sci. Instrum.* **2002**, 73, 1809-1812

(24) Treloar, L. *Polymer* **1960**, *1*, 95-103

(25) Treloar, L. *Polymer* **1960**, *1*, 279-289

(26) Oca, H.; Ward, I.; Klein, P.; Ries, M.; Rose, J.; Farrar, D. *Polymer* **2004**, *45*, 7261-7272

(27) Nishino, T.; Takano, K.; Nakamae, K. *Polymer* **1995**, *36*, 959-961

(28) Sato, H.; Miyada, M.; Yamamoto, S.; Reddy, K.; Ozaki, Y. *RSC Adv.* **2016**, *6*, 16817–16823

(29) Yu, C.; Bao, J.; Xie, Q.; Shan, G.; Bao, Y.; Pan, P. *CrystEngComm* **2016**, *18*, 7894-7902

CHAPTER II

Preparation and Mechanical Properties of Highly Oriented Poly (Glycolic Acid) Nanofibers

2.1 Introduction

Poly(glycolic acid)(PGA, -(CH2COO)m-) possess biocompatibility, biodegradability, hydrolyzability, and high mechanical properties. However, PGA had been used in limited field due to difficulty in mass production, such as biomedical applications such as sutures, bone fixation devices, and drug delivery carriers [1-5]. Recently, PGA has succeeded to develop the skill to mass production, then it will be expected to be useful high performance material more in the future.

Drawing process is effective method to make film or fiber oriented. After drawing then annealing, materials show well oriented and well crystallized, from amorphous state to crystalline state. However, PGA has been reported to be hard drawing polymer because of fast crystallization. If PGA can be drawn, it is expected to show higher mechanical and thermal properties.

In a past few decades, nanoscale materials are the subject of extensive worldwide researches. Because of their novel functionality and high performance, nanoscale materials were used not only academia but also many different types of applications within the textile, aerospace industry and so on. Nanoscale fibers (nanofibers) show high specific surface area and low structural defects. Electrospinning (ES) is well known as a low cost but effective method to produce polymer nanofibers [6-10]. It is a unique approach using electrostatic forces to produce fibers from polymer solutions or molten polymers, and the spun nanofibers possess a smaller diameter and larger surface area than those obtained from conventional spinning process. Thus, ES became well-recognized method and has already created interesting applications in drug delivery system, wound dressing, scaffolds in tissue engineering, and sensors in electronics [11-14]. In general,

ES is used to make nonwoven fabric.

Here, it is basically used ES technique but there is one distinguished different point in this study. Instead of using flat plate collector, used a rotating drum collector, which make fibers well-aligned. Then, aligned PGA nanofibers could be uniaxially drawn under heating to promote crystallization and uniaxial molecular orientation, which is expected to result in higher mechanical properties.

In this study, we prepared PGA nanofibers using electrospinning with rotating drum collector to align fibers. As spun PGA nanofibers were then drawn and annealed in order to well-orient and well-crystallize the nanofibers. We investigated the relationship between structure and mechanical properties of PGA nanofibers.

2.2. Experimental

2.2.1. Materials

PGA pellets were kindly supplied from KUREHA CORPORATION (KUREDUX B35®). PGA pellets were hot-pressed at 523 K, following by quenching into ice water, in order to make PGA film, first. PGA films are well dissolved in solvent than PGA pellets, due to the difference crystallinity and surface area, so make the film first and then dissolved. PGA films were dissolved in hexafluoro isopropanol (HFIP, Nacalai Tecque, Inc.) at room temperature overnight.

2.2.2. Sample preparation

For getting PGA cast film as a reference, PGA / HFIP solution (9 wt%) was cast in petri dish, then dried for 48 h at room temperature. PGA nanofibers were electrospun using rotating drum collector (MECC, Ogori, Japan, Figure 2.1.a)). The distance between the needles tip and collector was 15 cm and the applied voltage over the gap was 15 kV. The ambient temperature and humidity were 20-25 ℃ and 20-40 %, respectively. Disposable needle (the inner diameter: 0.44 mm) was used. PGA solution (9 wt%) was fed by syringe pump with flow rate of 1.0 mL/h. Electrospun fibers were collected onto rotation drum collector whose diameter was 20 cm with the rotating speed of 1000 rpm. These collected PGA nanofibers were aligned. Then, PGA nanofibers could be drawn 4 times at 50 ℃ with drawing rate of 1 cm/min, with 1 cm the initial length of PGA nanofibers. After drawing, PGA nanofibers were annealed at 110 ℃ for 30 min with the constant length (Figure 2.1.b)).

2.2.3. Characterization

Scanning electron microscope (SEM) observation was performed to study the surface morphology of nanofibers with a JSM-5610LSV (JEOL Ltd., Japan), at an accelerating voltage of 15 kV. Pt/Pd was deposited on the surface prior to the observation.

X-ray fiber photographs were taken using the CuKα radiation at 40 kV, 20 mA. The X-ray beam was irradiated perpendicular to the nanofibers. Exposure time was 30 min.

The tensile test was conducted using a tensile tester (Autograph AGS-1kND (Shimadzu Co.)) with a cross head speed of 1 mm/min. More than five specimens were tested with the initial length of 10 mm. The cross-sectional area was determined from the density

(floatation method with tetrachloromethane / benzene system at 30 ℃), weight and length. The Young's modulus was calculated by initial inclination of stress-strain curves with the same method described in Chapter 1.

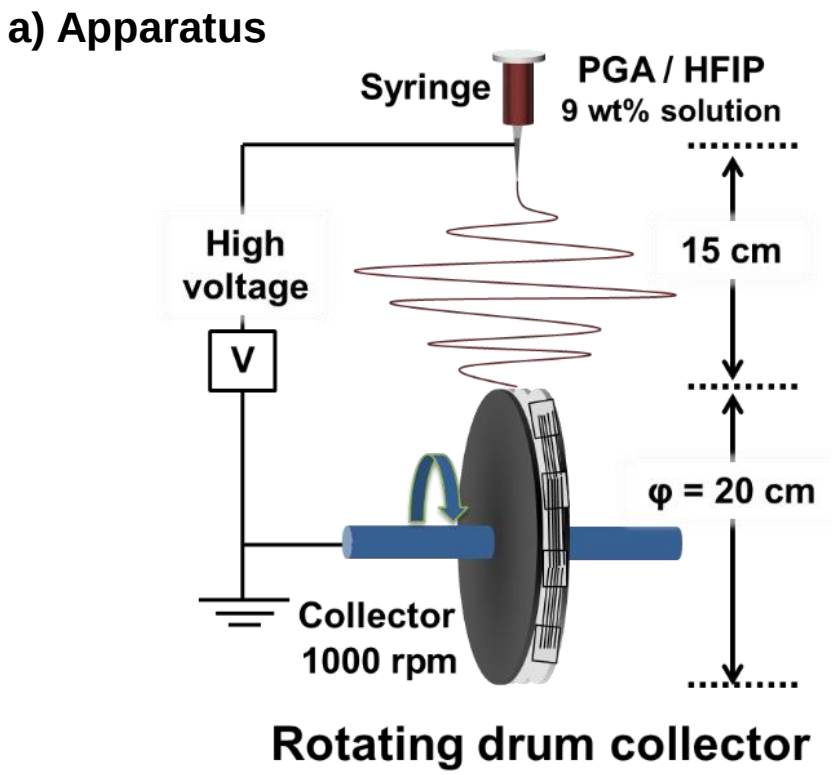

Fig. 2.1 a) Apparatus of electrospinning and b) schematic process of drawing and annealing of PGA nanofibers.

2.3. Results and Discussion

2.3.1. Nanofibers

Figure 2.2 show SEM images of as spun nanofibers and drawn & annealed nanofibers of PGA. PGA as spun nanofibers were smooth and well-aligned by optimizing spinning conditions such as voltage, solution feed rate and rotational speed of the drum collector. The fiber diameter was approximately 1.3 μm for as spun nanofibers. After drawing 4 times and annealing, the diameter became approximately 800 nm.

Figure 2.3 shows X-ray diffraction profiles and X-ray fiber photographs of cast film, as spun nanofibers and drawn & annealed nanofibers of PGA. For the PGA cast film, the reflection appeared as amorphous and an isotropic and diffuse scattering, indicating the cast film was not aligned, neither oriented. On the other hands, as spun PGA nanofibers showed two sharp peaks and ring-like diffuse scattering, indicating partially crystallized but randomly oriented. Furthermore, drawn & annealed PGA nanofibers revealed the sharper peaks than as spun nanofibers and well oriented crystalline reflections on the

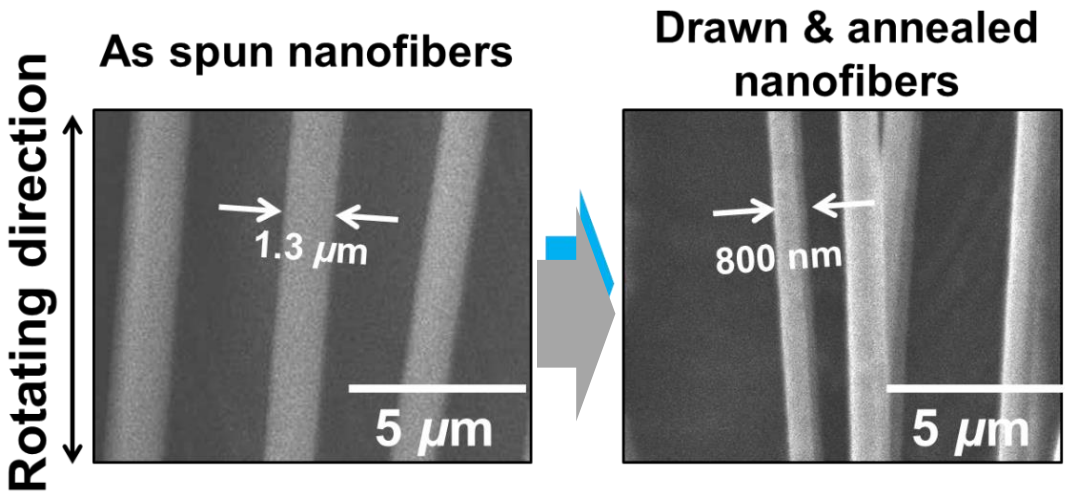

Fig. 2.2 SEM images of as spun nanofibers and drawn & annealed nanofibers of PGA.

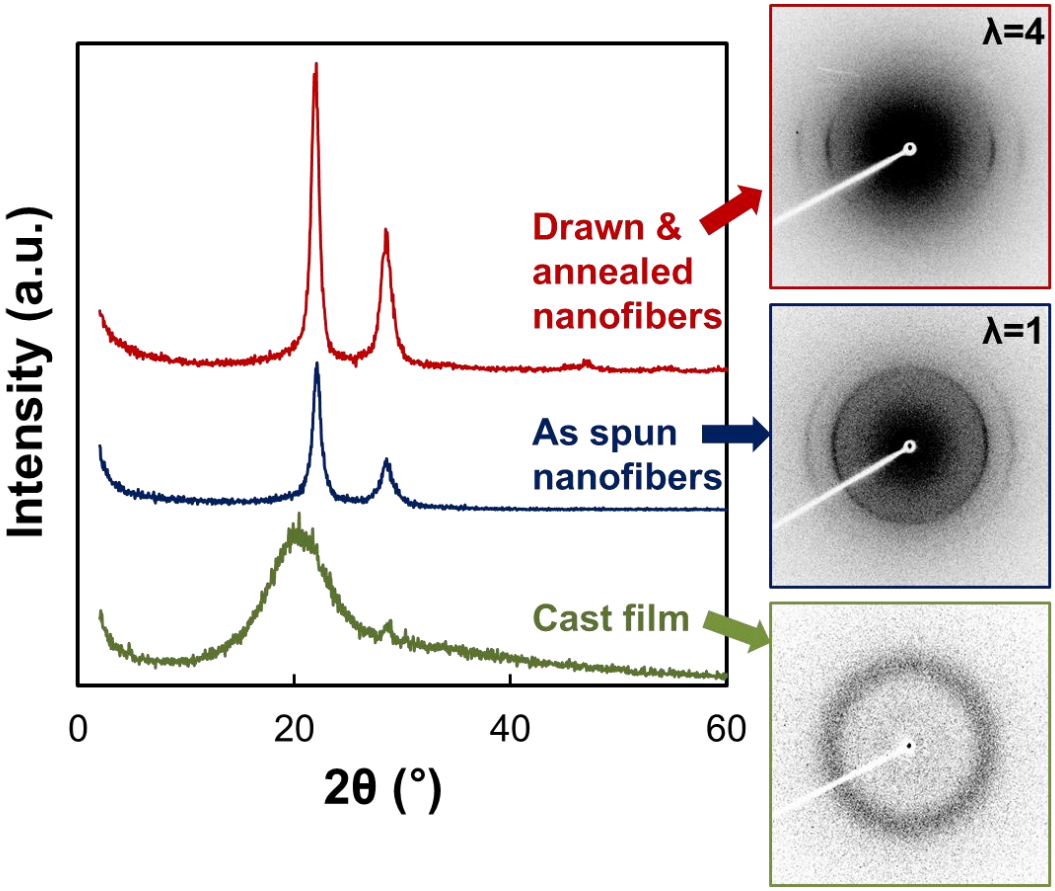

Fig. 2.3 X-ray diffraction profiles and X-ray fiber photographs of cast film, as spun nanofibers and drawn & annealed nanofibers of PGA.

equatorial direction. These suggest that PGA molecular chains were well packed and the crystallites were oriented by the drawing and annealing.

The degree of crystallite orientation (Π) of PGA as spun nanofibers and drawn & annealed nanofibers were evaluated by following equation (2.1).

$$\pi = (180 - H^{\circ})/180 \qquad (2.1)$$

where, H° is the peak width at half maximum in the intensity distribution profile along the Debye-Scherrer ring. The degree of the crystallite orientation was 0.88 for the 110 reflection for as spun nanofibers. This increased to 0.98 for drawn & annealed nanofibers.

It shows high crystallite orientation was attained by increasing draw ratio.

2.3.2. Mechanical properties

Figure 2.4 show stress-strain curves of cast film, as spun nanofibers and drawn & annealed nanofibers of PGA. Young's modulus (Y_l), tensile strength (σ_{max},) and elongation at break (ε_{max}) were summarized in Table. First, Y_l and σ_{max},of PGA as spun nanofibers

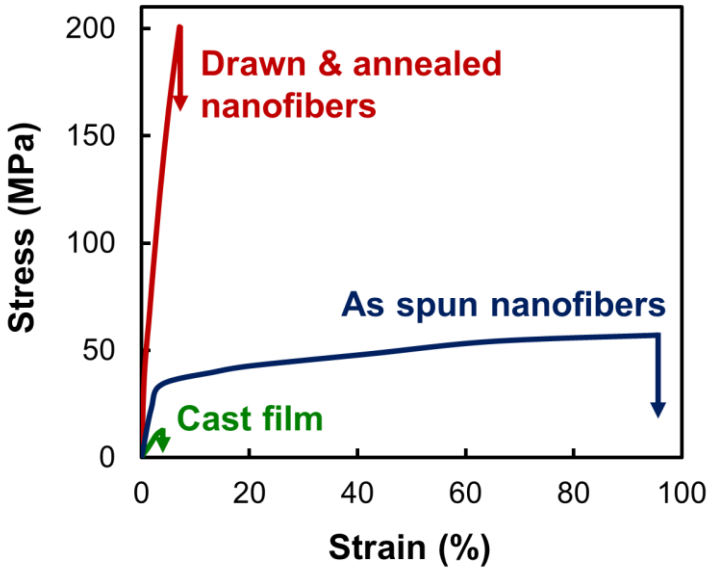

PGA	Y_l GPa	σ_{max} MPa	ε_{max} %
Cast film	0.5	13	3.8
As spun nanofibers	1.3	57	95.5
Drawn & annealed nanofibers	6.8	201	7.0

Fig. 2.4 Stress-strain curves and mechanical properties (Young's modulus (Y_l), maximum stress (σ_{max}), maximum strain (ε_{max})) of cast films, as spun nanofibers and drawn & annealed nanofibers of PGA.

were found to be 2.6 times and 4.3 times higher than those of PGA cast film, respectively. It is due to nano size effects, that is, high surface area and less defects in nanofibers.

Second, drawn & annealed nanofibers showed higher Y_l and σ_{max}, which were found to be 5.2 times and 3.5 times higher than those of PGA as spun nanofibers, respectively. In usual, polymer show higher mechanical properties after drawing and annealing, because of highly properties after drawing and annealing, because of highly orientation and high crystallinity.

Figure 2.5 show Normalized values of Young's modulus, tensile strength and elongation at break of cast films, as spun nanofibers and drawn & annealed nanofibers of PGA. The drawn & annealed nanofibers increase Y_l for 13.6 times and σ_{max} for 15.4 times, compared with cast film, respectively. Using rotating drum collector, PGA nanofibers were well

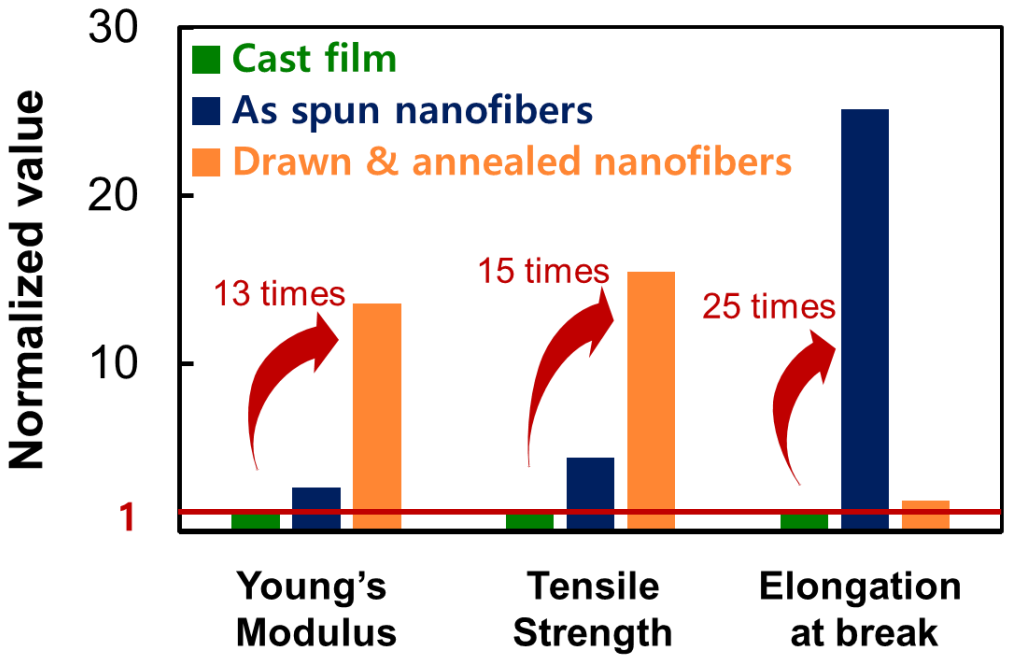

Fig. 2.5 Normalized values of Young's modulus, tensile strength and elongation at break of cast films, as spun nanofibers and drawn & annealed nanofibers of PGA.

aligned, and then drawing & annealing nanofibers become well oriented and crystallized. In addition, compared with cast film, the PGA nanofibers increase ε_{max} for 25 times. This suggest that the PGA nanofibers prepared by electrospinning could control the properties for the needs, such as high mechanical properties or flexibility.

Figure 2.6 show relationship between the crystallite orientation and Young's modulus (Y_l) of cast film, as spun nanofibers, and drawn & annealed nanofibers. The orientation (○) was calculated by equation (2.1), then normalized to percent (%). The Y_l (▲) increased with increasing the orientation. The orientation drastically increased for as spun

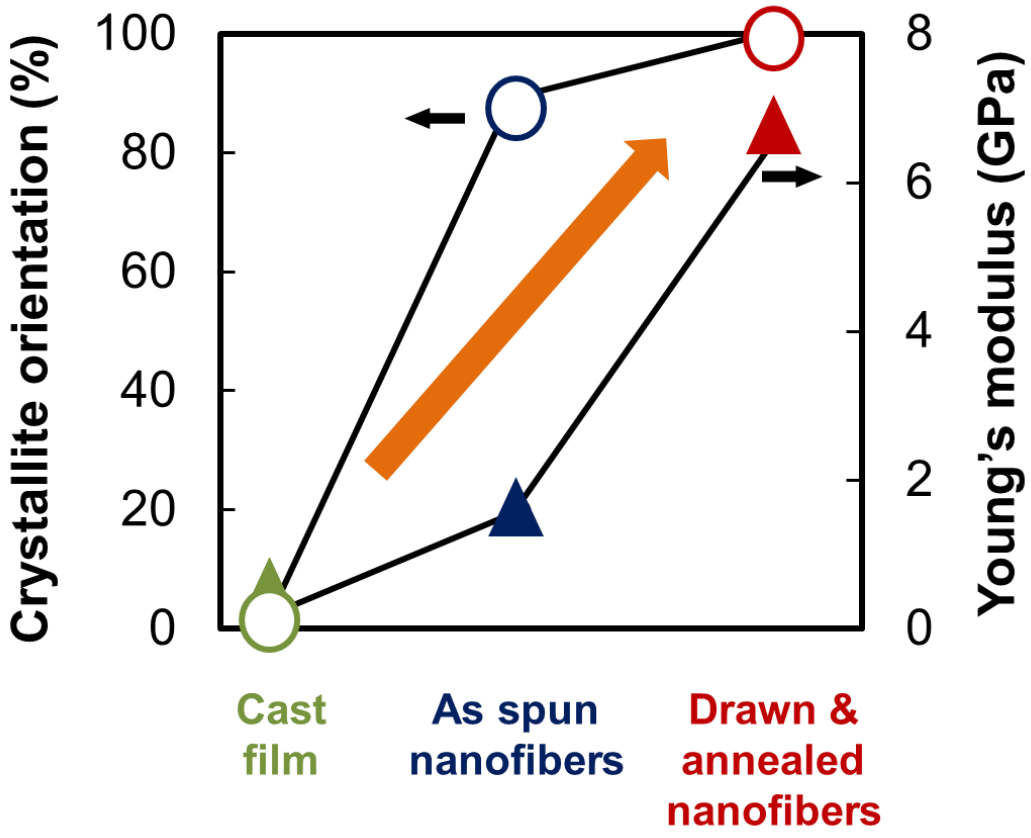

Fig. 2.6 Relationship between (○) orientation and (▲) Young's modulus of cast film, as spun nanofibers, and drawn & annealed nanofibers.

nanofibers compared with cast film, however, the Y_l value was not as much as increasing of the orientation. This suggest that the effect of amorphous regions governed the Y_l value more than that of crystallite orientation for as spun nanofibers. On the other hands, compared with as spun nanofibers, Y_l value of drawn & annealed nanofiber increased remarkably, though the orientation increase was only few %. Polymers were more oriented and crystallized by drawing and annealing process. Though, the mechanical properties of PGA nanofibers could not reach to maximum modulus, only as 7 %, however, this Young's modulus resemble that of electrospun/ drawn *it*.PP nanofibers [15]. Therefore, PGA nanofibers are expected to be used as an alternative material in many fields which requires the same modulus of *it*.PP.

2.4. Conclusions

PGA nanofiber was electrospun with the use of rotating drum collector to align nanofibers. Aligned nanofibers could be drawn 4 times, then annealed. The drawn and annealed PGA nanofibers showed not only high orientation (X-ray fiber photograph), but also high mechanical properties (tensile test) compared with those of cast film. As a results, drawn & annealed nanofibers show high Young's modulus (6.8 GPa), tensile strength (201 MPa). Both the crystallite orientation and mechanical properties were found to be increased by drawing & annealing of PGA nanofibers. This Young's modulus of PGA resemble that of electrospun/ drawn *it*.PP nanofibers, therefore, PGA nanofibers are expected to be used as an alternative material in many fields which requires the same modulus of *it*.PP.

2.5. References

(1) Lee, S.; Hongo, C.; Nishino, T. *Macromolecules* **2017**, *50* (13), 5074–5079

(2) Chatani, Y.; Suehiro, K.; Ô kita, Y.; Tadokoro, H.; Chujo, K. *Die Makromol. Chemie* **1968**, *113* (1), 215–229

(3) Gilding, D. K.; Reed, A. M. *Polymer* **1979**, *20* (12), 1459–1464

(4) Yamane, K.; Sato, H.; Ichikawa, Y.; Sunagawa, K.; Shigaki, Y. *Polym. J.* **2014**, *46* (11), 769–775

(5) Sekine, S.; Akieda, H.; Ando, I.; Asakura, T. *Polym. J.* **2008**, *40* (1), 10–16

(6) Bhardwaj, N.; Kundu, S. C. *Biotechnol. Adv.* **2010**, *28* (3), 325–347

(7) Huang, Z. M.; Zhang, Y. Z.; Kotaki, M.; Ramakrishna, S. *Compos. Sci. Technol.* **2003**, *63* (15), 2223–2253

(8) Kakade, M. V.; Givens, S.; Gardner, K.; Lee, K. H.; Chase, D. B.; Rabolt, J. F. *J. Am. Chem. Soc.* **2007**, *129* (10), 2777–2782

(9) Doshi, J.; Reneker, D. H. *J. Electrostat.* **1995**, *35* (2–3), 151–160

(10) Greiner, A.; Wendorff, J. H. E. *Angewandte Chemie - International Edition*. 2007, pp 5670–5703.

(11) Gensheimer, M.; Becker, M.; Brandis-Heep, A.; Wendorff, J. H.; Thauer, R. K.; Greiner, *Adv. Mater.* **2007**, *19* (18), 2480–2482

(12) Tsuji, H.; Nakano, M.; Hashimoto, M.; Takashima, K.; Katsura, S.; Mizuno, A. *Biomacromolecules* **2006**, *7* (12), 3316–3320

(13) Khil, M.-S.; Cha, D.-I.; Kim, H.-Y.; Kim, I.-S.; Bhattarai, N. *J. Biomed. Mater. Res.* **2003**, *67B* (2), 675–679

(14) Ding, B.; Wang, M.; Yu, J.; Sun, G. G. *Sensors* **2009**, *9* (3), 1609–1624

(15) Nishino, T.; Asahina, Y.; Hongo, C. All Polypropylene Nanocomposite With Well-Aligned and Well-Oriented. *20th Int. Conf. Compos. Mater.* **2015**, No. July, 19–24.

CHAPTER III

Elastic Modulus of the Crystalline Regions of Poly (Lactic Acid)

3.1 Introduction

Among bio based polymers, poly(lactic acid)(PLA, -$(CH_2CH(CH_3)COO)_n$-) is the most popular biodegradable bio based aliphatic polyester obtained by fermenting corn starch or sugar cane [1-3], and is synthesized by ring-opening polymerization of lactide. PLA has biocompatibility and hydrolyzability. PLA is very attractive for using not only in industrial fields, but also in biomedical applications, e.g., sutures, bone fixation, or drug delivery systems [4-9].

Ikada *et al.* discovered same amount of solution blend of poly(L-lactic acid) (PLLA) and poly(D-lactic acid) (PDLA) crystallized as stereocomplex in 1987 [10]. Since then, many procedures for making stereocomplex PLA (scPLA) from PLLA and PDLA, such as by solution blend, in a solid state blend from the melt, during polymerizations, were reported [11-12]. scPLA is known to show different structure and properties from PLAs. For example, scPLA shows higher melting point (~230 °C) than that (~180 °C) of PLAs. The unit cell of PLAs belongs to pseudo orthorhombic crystal system, which changes into triclinic system when stereocomplexation occurs [11]. PLLA and PDLA are reported to possess 10_3 helical conformation in the crystal lattice. On the contrary, scPLA possesses 3_1 helical conformation, similar to isotactic polypropylene (*it*.PP) [13].

Crystal modulus is one of the most important mechanical properties of polymers. The crystal modulus E_l and E_t have been measured by X-ray diffraction [14-17]. The data so far accumulated show the E_l value gives us information about the skeletal conformation, deformation mechanism, and maximum modulus for the specimen modulus of polymers. The E_l values for polymers with fully extended planar zigzag conformation, such as polyethylene (PE) is 235 GPa, whereas *it*.PP (helical structure) show the E_l value of 33

GPa. This low E_l value of *it*.PP is due to that helical skeleton is easy to elongate to the stress direction compared with the planar zigzag one. On the other hand, the E_t values are correlated with the intermolecular interactions such as van der Waals force, dipole-dipole interaction, and hydrogen bonding, together with their anisotropies.

The crystal modulus of poly(L-lactic acid) (PLLA) was evaluated experimentally and theoretically [18-19]. However, only the crystal modulus of PLLA along the chain direction at room temperature is insufficient for overviewing the relationship between structure and properties of a series of PLA. For example, as mentioned above, the melting point of scPLA is more than 50 degree higher than those of PLLA and PDLA. However, no reasonable explanation on this phenomenon was described in the literatures. Intermolecular hydrogen bonding between CH_3 and C=O was proposed for PLLA by Ozaki *et al.* [20], but no information was available on the strength of intermolecular interaction of PLAs. In order to investigate these unsolved issues from the mechanical point of view, crystal modulus of not only PLLA, PDLA, but also that of scPLA, including their crystal modulus both in the directions parallel and perpendicular to the chain axis was evaluated. In addition, temperature dependence of the crystal modulus of PLLA, PDLA, and scPLA were also investigated in this study to examine the thermal properties of the crystalline regions of PLAs.

3.2. Experimental

3.2.1. Sample preparation

PLLA pellets were kindly supplied from Unitika a Ltd. (4032DK), and PURASORB®

for PDLA. Molecular weight of PLLA was 4.5 x 10^4 for number average molecular weight (M_n), 9.5 x 10^4 for weight average molecular weight (M_w). The M_n, M_w of PDLA were 1.1 x 10^5 and 1.5 x 10^5, respectively. The M_n, M_w were measured by gel permeation chromatography using chloroform as an eluent, and used polystyrene (PS) for standards. The pellets were hot-pressed at 453 K, followed by slowly cooling to room temperature. PLLA and PDLA film (thickness : 90 μm) was uniaxially drawn 6 times its original length at 348 K, then annealed at 408 K for 0.5 h at the constant length. In addition, highly oriented and highly crystallized PLLA by solid state extrusion (K-PLLA), kindly supplied from prof. T. Kanamoto in Science University of Tokyo, was also used for the crystal modulus measurement [21].

scPLA film was prepared by solution cast on glass petri dish, with the same weight ratio mixture of PLLA and PDLA dissolved in chloroform for each 1.5 wt%. Transparent film was successfully peeled off from the substrate. Film was dried for 3 d at room temperature to remove solvent. The film (thickness : 28 μm) was drawn 6 times its original length at 363 K, then annealed at 483 K for 1 h at the constant length.

3.2.2. Characterization

The tensile properties measurement of drawn and annealed PLLA, PDLA and scPLA films were basically same method with those in Chapter 1. Calculation of the cross-sectional area for PLLA, PDLA and scPLA was evaluated from the reported density (1.24 g/cm^3 [22]), and measured weight and length of the sample.

The melting point (T_m) and enthalpy of fusion (ΔH) of PLLA, PDLA and scPLA were

the same with those of Chapter 1. But, a sample weight was approximately 3 mg.

Crystallinity X_c of PLLA, PDLA and scPLA were evaluated with the following equation (3.1).

$$X_c = \Delta H / \Delta H_0 \tag{3.1}$$

where ΔH_0 (PLLA and PDLA) = 93 J/g [23], ΔH_0 (scPLA) = 146 J/g [24], for 100 % crystallinity.

X-ray diffraction photographs were recorded on an imaging plate that had a camera length of 58 mm, with the same method as those of Chapter 1.

To obtain the crystallite size D_{hkl}, the observed profiles for the (*hkl*) planes were according to the Chapter 1 equation (1.2) and equation (1.3).

The degree of the crystallite orientation π was defined by the equation (3.2)

$$\pi = (180 - H^\circ)/180 \tag{3.2}$$

where H° is the half-width of the intensity distribution curve for the equatorial 200/110 reflection for PLLA, PDLA and 100/010/1-10 reflection for scPLA along the Debye-Scherrer ring.

3.2.3. Elastic Modulus of the Crystalline Regions

The strain ε and the stress σ in the crystalline regions by X-ray diffraction, crystal modulus E_l and E_t and their temperature dependence from cryogenic temperature to high temperature were measured and calculated with the same method described in Chapter 1.

3.3. Results and Discussion

3.3.1. Sample Characteristics

Figure 3.1 shows X-ray fiber photographs of drawn and annealed PLLA, PDLA and scPLA film at 300 K. All samples were highly crystallized and the crystallites were highly oriented along the drawn direction. The fiber photographs of PLLA and PDLA were that of typical α-form, which were completely different from that of scPLA. We confirmed the scPLA film contained only scPLA, as no more PLLA and PDLA peak appeared on

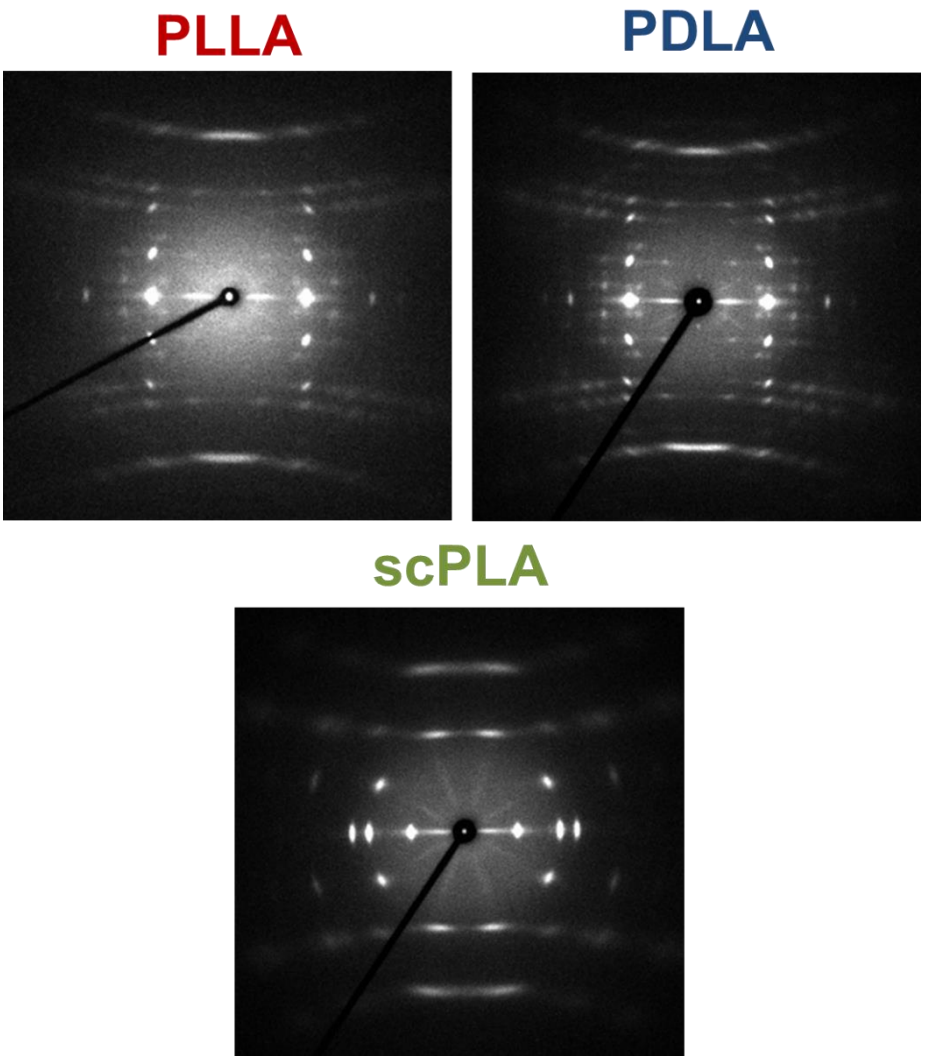

Fig. 3.1. X-ray fiber photographs of PLLA, PDLA and scPLA.

the fiber photograph.

Figure 3.2 show X-ray fiber photograph and meridional X-ray diffraction profile of PLLA film (K-PLLA) supplied from Kanamoto Laboratory. From the figure, K-PLLA possessed extremely high crystallite orientation, crystallinity, low lattice disorder, and α-form was only appeared, too.

Figure 3.3 shows (upper) meridional and (lower) equatorial X-ray diffraction profiles of drawn and annealed PLLA, PDLA and scPLA film at 300 K. On the basis of the reported crystal lattice of PLLA and PDLA (orthorhombic, a = 10.6 Å , b = 6.1 Å , c (fiber axis) =

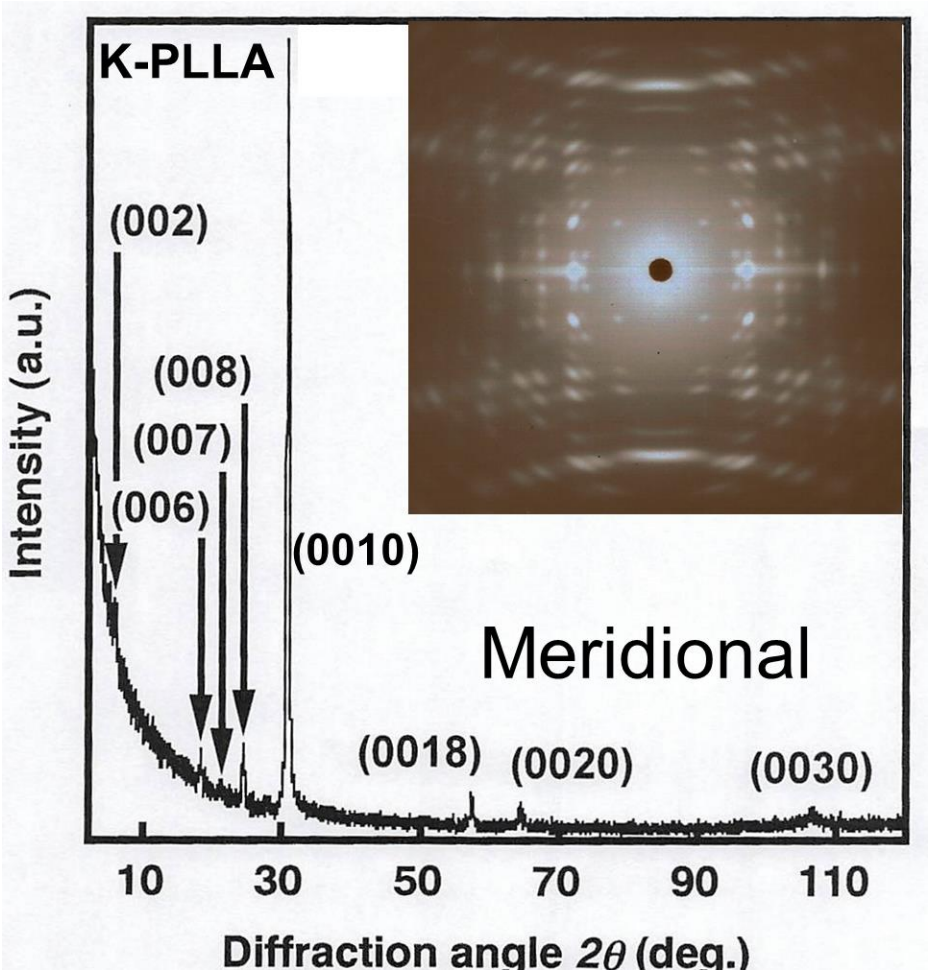

Fig. 3.2 X-ray fiber photograph and meridional X-ray diffraction profile of PLLA film (K-PLLA) supplied from Kanamoto Laboratory.

28.8 Å) [25] and scPLA (triclinic, a = 9.16 Å , b = 9.16 Å , c (fiber axis) = 8.7 Å , α,β = 109.2 °, γ =109.8 °) [13], the diffraction peaks could be indexed as shown in the figure, respectively. Meridional 0010 reflection for PLLA and PDLA, -2-26 reflection for scPLA were used to measure the E_l values. The normal of the -2-26 reflection is inclined at an angle of 1.3 ° from the meridian. This angle coincides with the angle expected from the

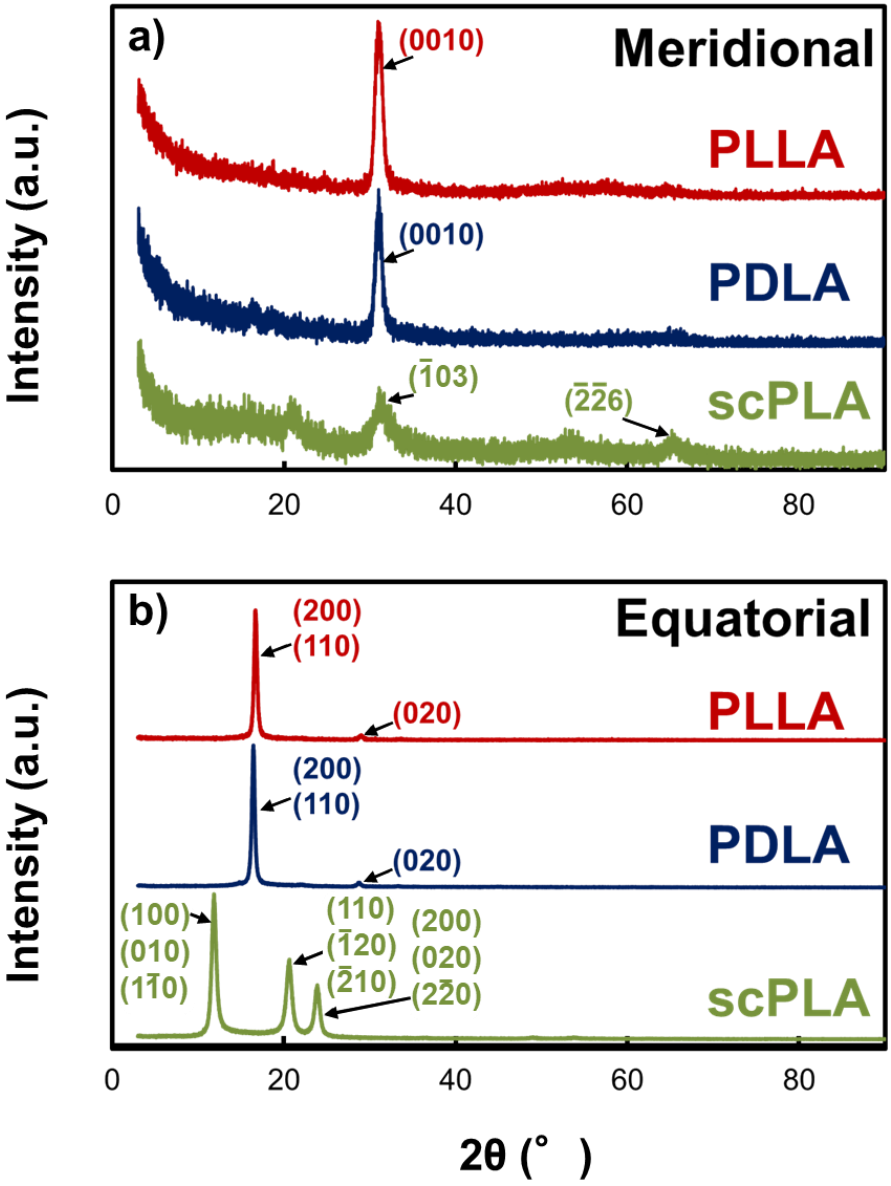

Fig. 3.3 a) Meridional and b) equatorial X-ray diffraction profiles of PLLA, PDLA and scPLA.

crystal structure. Therefore, in fact for crystal modulus measurement, the inclination correction should be needed. However, σ and ε were not corrected for the inclination of this lattice plane, because it is negligibly small [26]. The E_t values were measured for 200/110 and 020 reflections for PLLA and PDLA, 100/010/1-10, 110/-120/-210, 200/020/2-20 reflections for scPLA, respectively.

Table 3.1 Sample preparation conditions (drawing, annealing), crystallite orientation, crystallinity, crystallite size, melting point T_m, Young's modulus Y_l, tensile strength σ_{max} and elongation at the break ε_{max} of PLLA, PDLA and scPLA.

	PLLA	PDLA	scPLA
Drawing	λ = 6 @75 °C		λ = 6 @90 °C
Annealing	@ 135 °C 0.5 h		@ 210 °C 1 h
Crystallite orientation	0.97	0.96	0.95
Crystallinity (%)	61	68	36
Crystallite size (Å)			
(0010)	88	104	
(-2-26)			57
T_m (°C)	165.3	180.9	214.1
Y_l (GPa)	6.2	5.8	5.6
σ_{max} (MPa)	128	179	108
ε_{max} (%)	43	48	19

Table 1 summarized sample preparation conditions (drawing, annealing), and characteristics (crystallite orientation, crystallinity, crystallite size, melting point T_m, Young's modulus Y_l, tensile strength σ_{max} and elongation at the break ε_{max}) of PLLA, PDLA and scPLA. Though PDLA showed a little bit larger crystallite size and higher melting point, PLLA and PDLA intrinsically showed same properties. Compared with PLAs, scPLA showed low crystallinity and small crystallite size, but it possessed higher mechanical properties and higher melting point (approximately 40 ℃).

3.3.2. Crystal modulus E_l

Figure 3.4 shows the stress σ - strain ε curves for the 0010 reflections of (○) PLLA and (□) PDLA together with that (▲) of K-PLLA at 300 K. All the plots could be expressed with a straight line with the same inclination through the origin, and the lattice extensions were always reversible. The initial inclination of this line gave the crystal modulus E_l of PLLA, PDLA and K-PLLA as 14 GPa at 300 K. Same crystal modulus E_l for PLLA, PDLA and K-PLLA even with different microstructures supports the homogeneous stress distribution.

As mentioned previously, the crystal modulus correspond to the maximum modulus, because the elastic modulus were measured by X-ray diffraction method where only the polymer crystallite were detected. Pennings *et al.* attempted to get high modulus / high strength fiber using PLLA [5]. They succeeded to increase strength up to 1 GPa, but the modulus remained low (<10 GPa). A lot has been tried for getting high modulus PLLA fiber, but failed [27-28]. As mentioned above, the reason for low macroscopic modulus of PLLA fiber can be attributed to low crystal modulus of PLLA, and so called high

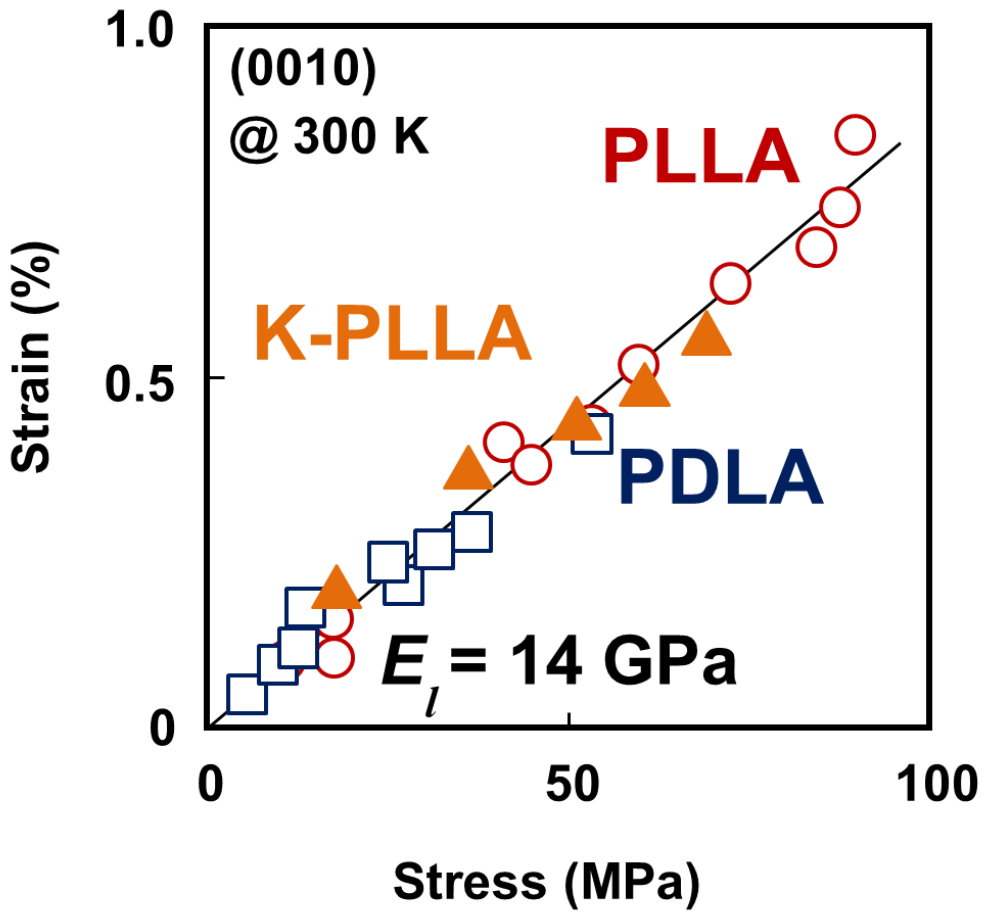

Fig. 3.4 Stress-strain curves for the (0010) plane of (○) PLLA, (□) PDLA and (▲) K-PLLA at 300K.

modulus fiber/film can not be obtained using PLLA and PDLA. In addition, PLLA is often applied in biomedical fields [8-9], but low crystal modulus also suggests that PLLA alone is not suitable for bone replacement, and some reinforcement will be needed for this purpose.

The observed E_l values (14 GPa) of PLAs are much lower than that (235 GPa) of PE with a fully extended planar zigzag conformation in the crystalline regions. If the PLA skeleton is assumed to be fully extended planar zigzag, the E_l value, evaluated by Treloar's method [29-30] using the reported bond lengths, bond angles and these force

constants (see Table S2), was 120 GPa, which is 8.6 times higher compared with the observed one.

De Oca *et al.*[18] calculated the crystal modulus of PLLA *α*-form, as 36 GPa, based on the lattice model proposed by Kobayashi *et al*.[31], in which two 10_3 helices are packed in the unit cell. However, Tashiro *et al.*[19] suggest their modulus calculation cannot be assumed to be satisfactorily exact since the crystal structure employed by them is not enough reasonable. On the contrary, Tashiro *et al.* calculated the E_l value for 10_3 helical *α*-form on the basis of the refined crystal structures of PLLA as 14.7 GPa. They also observed the E_l value for PLLA *α*-form as 13.76 GPa, which coincided with the E_l value in this study. We here confirmed the linearity of σ- ε curve up to higher σ both for PLLA, PDLA (Figure 3.4) with wide variety of microstructure, compared with the previous one ($\sigma < 60$ MPa) [19] . This supports higher reliability of the results in the present study.

As mentioned in introduction, helical skeleton gives low E_l value than that of planar zigzag one. The contraction of 10_3 helical structure is calculated as approximately 20 % from planar zigzag conformation in the crystalline regions [32]. The bigger contraction brings the smaller the E_l value. Therefore, the low E_l value of PLLA and PDLA will be explained by helical skeleton in the crystalline regions.

Figure 3.5 the σ-ε curve for the -2-26 reflections of scPLA, together with the results of figure 3.4 expressed with the dotted line, at 300 K. All the plots could be expressed with a straight line with the same inclination through the origin, and the lattice extensions were always reversible. The initial inclination of the line gave the crystal modulus E_l of scPLA as 20 GPa at 300 K. This is higher as 140 % compared with those of PLLA and PDLA. Okihara *et al.*[13] proposed the crystal structure of scPLA, as 3_1 helical conformation.

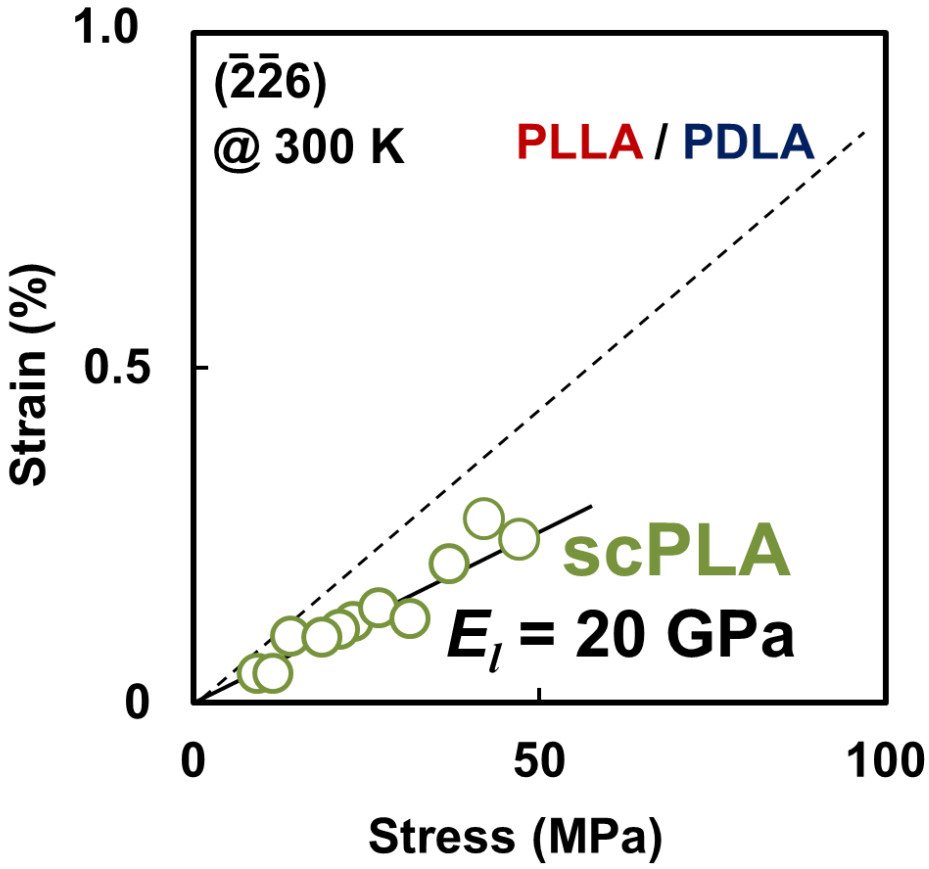

Fig. 3.5 Stress-strain curves for the (○) (2̄2̄6) plane of scPLA at 300K. Broken line represent the results of Fig.3.4 for comparison.

This slightly extended conformation (3_1 helix) brings scPLA become hard to extend (elongation) characteristic to scPLA skeleton. Therefore, 3_1 helix (scPLA) shows higher E_l value compared with that 10_3 helix (PLLA and PDLA).

Figure 3.6 shows the stress-strain curves for the (0010) plane of (○) PLLA and (□) PDLA, (-2-26) plane of (○) scPLA at various temperature. The E_l values were evaluated from the initial inclination of each curve at each temperature.

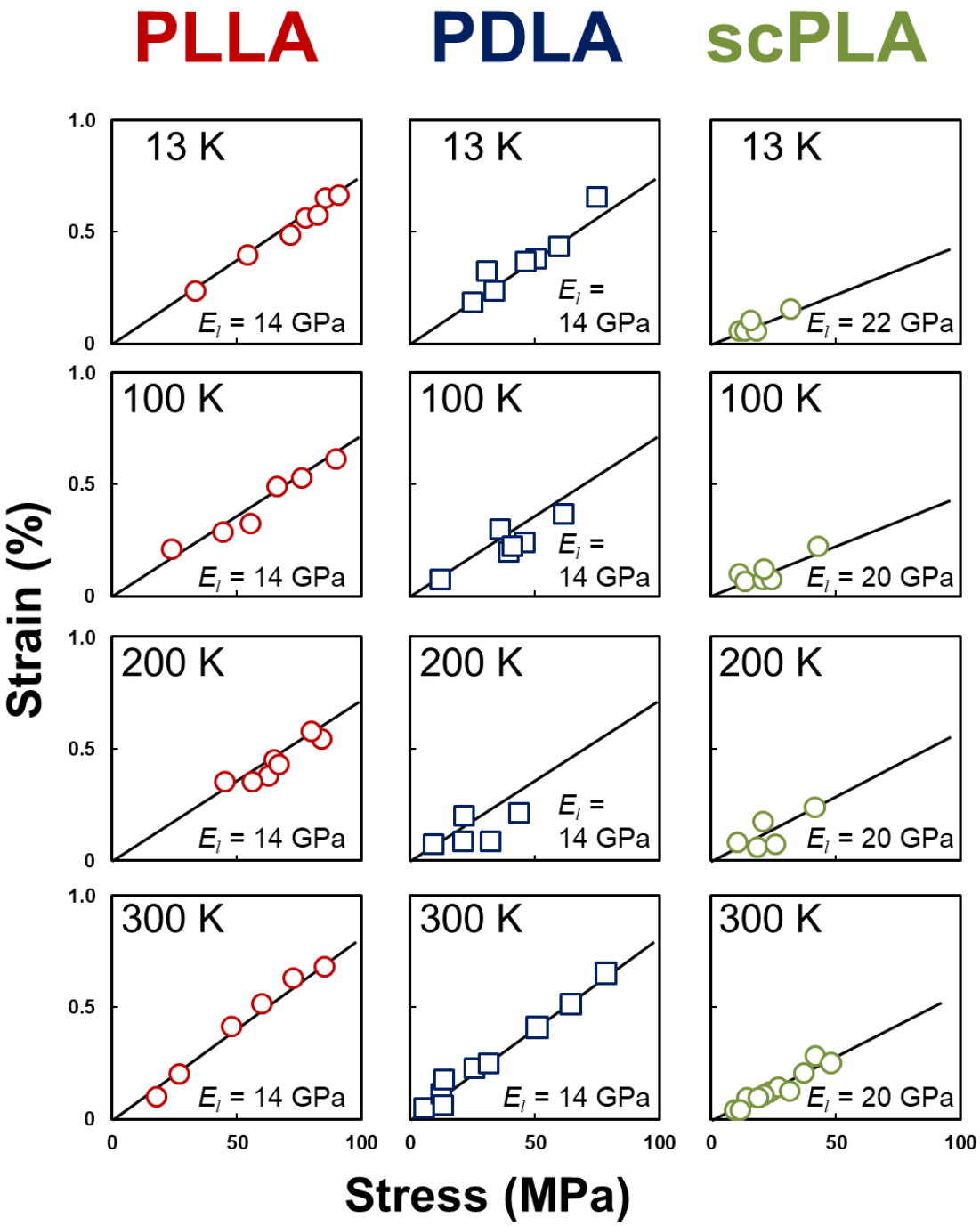

Fig. 3.6 Stress-strain curves for the (0010) plane of (○)PLLA and (□) PDLA, (226) plane of (○) scPLA at various temperature.

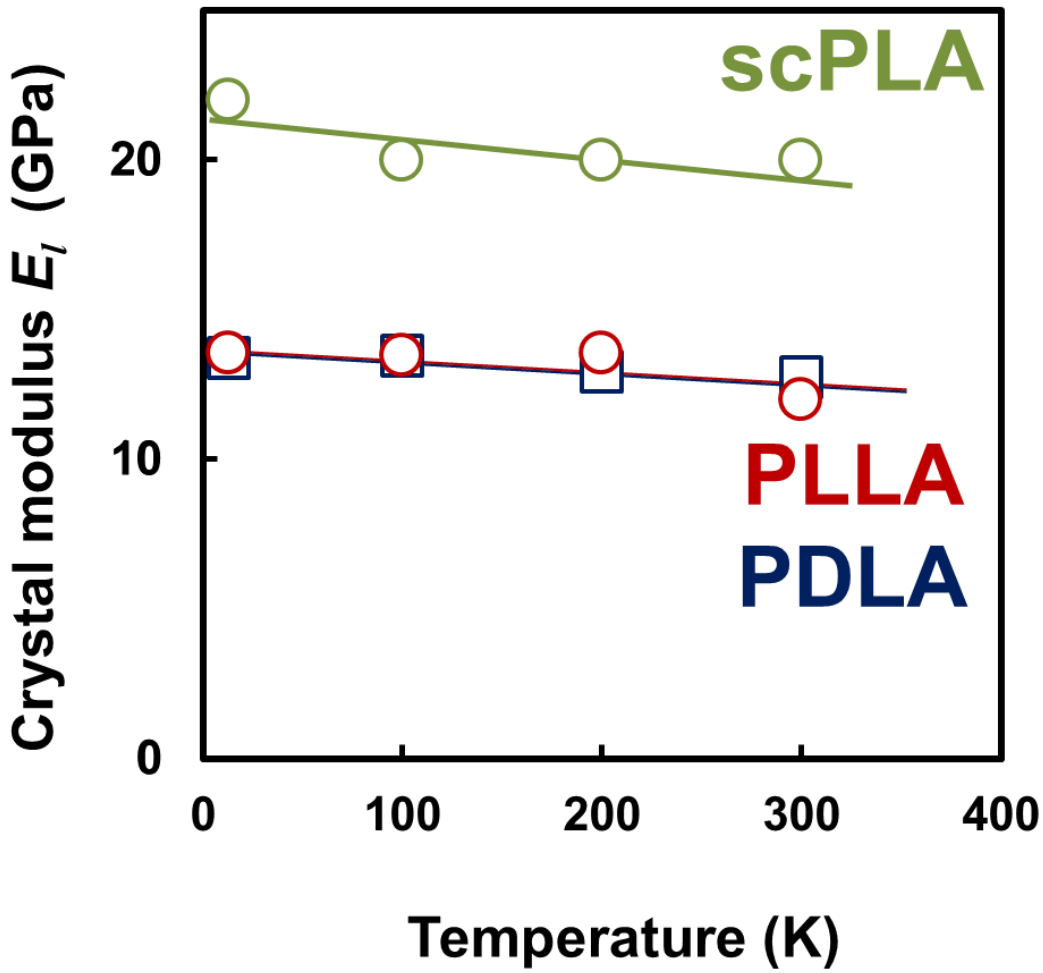

Fig. 3.7 Relationship between temperature and crystal modulus E_l for the (0010) plane of (○) PLLA, (□) PDLA and (○) ($\bar{2}\bar{2}6$) plane of scPLA.

Figure 3.7 shows the relationship between temperature and the crystal modulus E_l for the (0010) plane of (○) PLLA, (□) PDLA and (-2-26) plane of (○) scPLA. The E_l values of PLLA and PDLA was 14 GPa at 13 K, which is the same at room temperature. For scPLA, the E_l value was 22 GPa at 13K, which is slight higher than that at room temperature. However, the E_l value of scPLA at cryogenic temperature can be said to be almost same as that of room temperature, considering the experimental error (±10 %). So it is suggested that PLAs and their stereocomplex are stable against the heat. These are in

the contrast with the results for PGA, where the E_l value of PGA show temperature dependence from cryogenic temperature to high temperature [33]. Even same C-O-C repeated unit in molecular chain, the difference between PLAs and PGA is due to that helical skeleton of PLAs is already largely contracted in the crystalline regions, and their structural effect surpasses the temperature effect.

3.3.3. Crystal modulus E_t

Figure 3.8 show the stress σ - strain ε curves for the equatorial (200/110), (020) planes of (○) PLLA, (□) PDLA and (100/010/1-10), (110/-120/-210), (200/020/2-20) planes of scPLA at 300 K, respectively. The curves for the equatorial reflections could be also expressed with a straight line through the origin, and the lattice extensions were always reversible. The E_t values of PLLA and PDLA were 3.2 and 2.8 GPa for the (200/110) and (020) planes at room temperature, respectively. These E_t values are smaller than that (4 GPa) of PE only based on van der Waals intermolecular interaction [16] or that (6.6 GPa) of poly(vinyl alcohol) (PVA) based on intermolecular hydrogen bonds [17]. Thus, these results suggest van der Waals intermolecular interactions mainly act in PLLA and PDLA molecules in the crystal lattice.

On the other hands, the E_t values of scPLA were 4.0, 4.6 and 4.1 GPa for (100/010/1-10), (110/-120/-210) and (200/020/2-20) planes at 300 K, respectively. These E_t values of scPLA are higher than those of PLLA and PDLA. These reveal scPLA possesses higher intermolecular cohesive energy compared with PLAs. Ozaki *et al.* [20] suggest there are hydrogen bonds of CH_3 …O=C, in the stereocomplex crystals. However, judging from

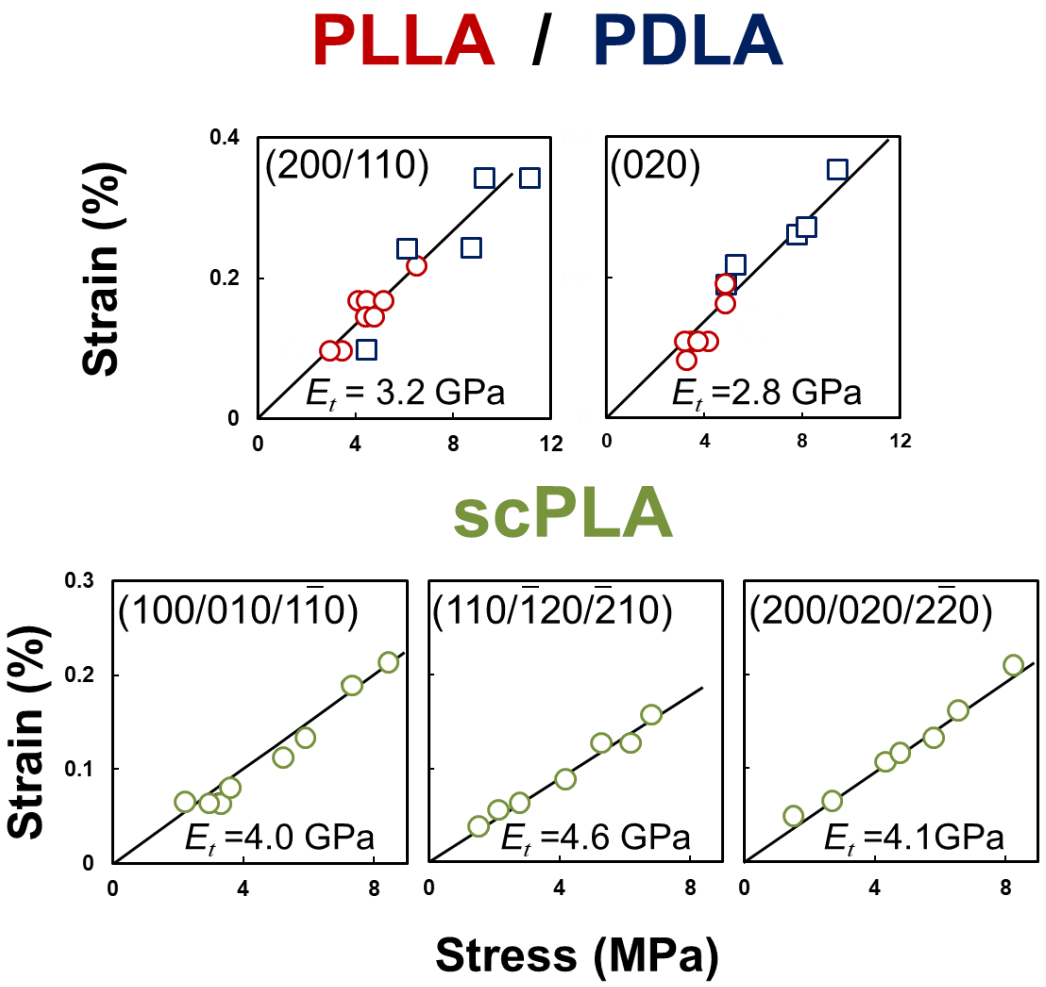

Fig. 3.8 Stress-strain curves for the equatorial planes of PLLA, PDLA and scPLA at 300 K.

the E_t values of scPLA (just same as PE, also much smaller than that of PVA or polyamides which possess hydrogen bonds), no strong hydrogen bonding acts from the mechanical point of view.

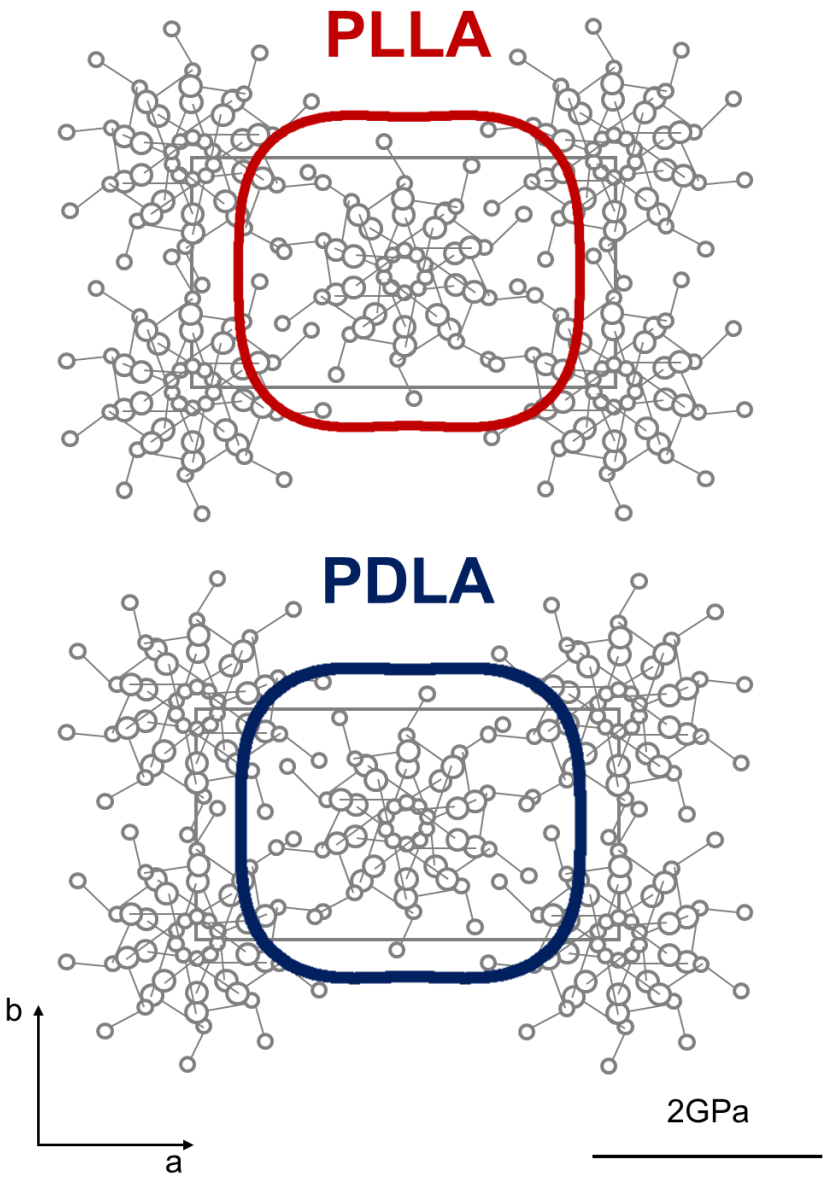

Fig. 3.9 Anisotropies of the E_t values in the *ab* plane of PLLA and PDLA at 300K.

Figure 3.9 shows anisotropy of the E_t value superimposed with the molecular packing in the *ab* plane of PLLA and PDLA at 300 K [13]. The anisotropies of the E_t values in PLLA and PDLA were calculated from the observed E_t values using following equation (3.3) [34].

$$1/E_\theta = cos^4\theta/\ E_0 + sin^4\theta/\ E_{90} + [1/\ G_{0,90} - 2(v_{0,90}/\ E_0)]sin^4\theta * cos^4\theta \qquad (3.3)$$

where E_θ is the E_t value at the angle of θ from a-axis, E_0 and E_{90} are E_t value along a- and b-axis, $G_{0,90}$ is shear modulus in a- and b- axis direction. $v_{0,90}$, Poisson's ratio was assumed to be 0.33 in the present study.

The E_t values are almost isotropic for PLLA and PDLA, and no difference between PLLA and PDLA even these possess opposite helical direction, respectively. Tashiro *et al.* [19] calculated the E_t values of PLA, and reported that they were almost comparable to that of PE, *it*.PP, but far below compared with those of PVA, Nylon6. In addition, calculated E_t value was almost isotropic in the ab plane. These calculation also coincide with the observed ones in Figure 3.9 and 3.10.

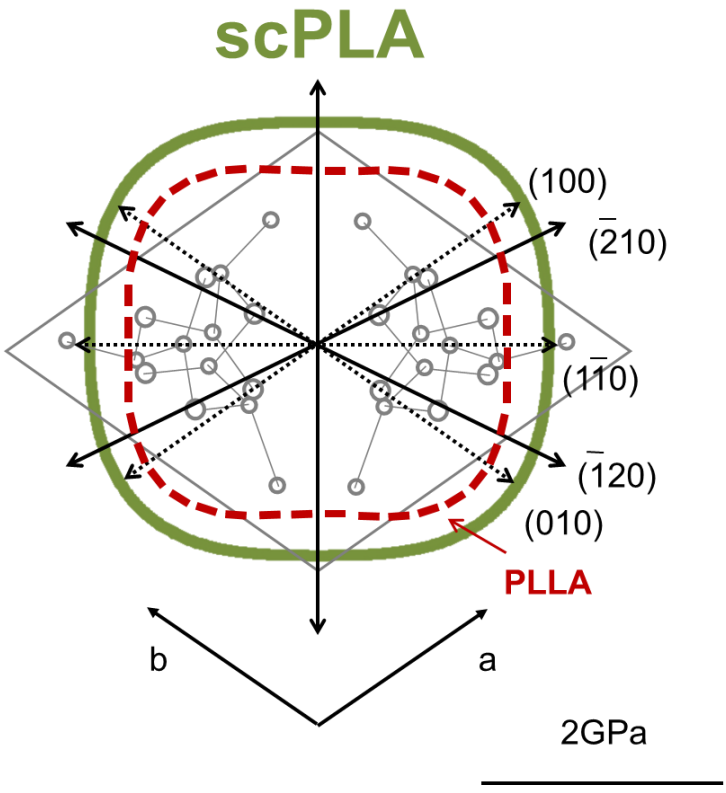

Fig. 3.10 Anisotropy of the E_t value in the *ab* plane of scPLA at 300K. The results in Fig.3.8 is superimposed with (-) the broken line at 300K.

Figure 3.10 shows anisotropy of the E_t values and the molecular packing of scPLA in the *ab* plane at 300 K [35], together with that of PLLA with the broken line for comparison. The unit cell contains one PLLA and one PDLA chain with shape of an equilateral triangle, and reported to be formed e quilateral-triangle-shaped single crystals of the scPLA [13][36]. The arrows express the E_t value corresponding to each directions. The E_t values of scPLA are almost isotropic as same trend as those of PLLA and PDLA [19]. However, compared with PLLA and PDLA, scPLA possess higher E_t values for all directions. These results indicate there are stronger intermolecular interaction between PLLA and PDLA molecular chains, compared in the cases between PLLA/PLLA, PDLA/PDLA combinations.

The melting point is defined as the ratio of the change in entropy of fusion (ΔS) and enthalpy of fusion (ΔH), ($T_m = \Delta H/\Delta S$). As discussed in the previous paper [33], the E_t values can be correlated with ΔH from mechanical point of view. The higher melting point (~230 ℃) compared with those (~180 ℃) of PLLA and PDLA can be attributed to higher E_t value of scPLA, in other words, higher intermolecular interaction of scPLA compared with those of PLLA and PDLA..

3.4. Conclusions

Crystal modulus of PLLA, PDLA and scPLA in the directions both parallel (E_l) and perpendicular (E_t) to the chain axis were measured by X-ray diffraction. PLLA and PDLA possesses same E_l value as 14 GPa, even though, they possess opposite chain helical direction, at room temperature. This small E_l value is caused by largely contracted 10_3 helical structure in the crystalline regions for PLLA and PDLA. The E_l value of scPLA is 20 GPa at room temperature, being higher than those of PLLA and PDLA. This is due to that the skeleton of scPLA is slightly extended (3_1 helix) than those of PLLA and PDLA. All PLLA, PDLA and scPLA showed temperature independence of the E_l values from cryogenic temperature to room temperature, which is considered that the structural effect on the E_l value is higher than the temperature effect. Even with the existence/ absence of methyl groups inserted on the side chain, the results of PLA was quite different from those of PGA [33]. The E_t values of PLLA and PDLA were smaller than that of PE. These suggest that only weak van der Waals intermolecular interactions act in PLLA and PDLA. The E_t value of scPLA was slightly higher than those of PE, PLLA and PDLA, however, they was lower than that based on hydrogen bonding.

3.5. References

(1) Tsuji, H. In *Poly(Lactic Acid)*; Auras, R., Lim, L.-T., Selke, S. E. M., Tsuji, H., Eds.; John Wiley & Sons, Inc.: Hoboken, NJ, USA, 2010; pp 343–381.

(2) Ikada, Y.; Tsuji, H. *Macromol. Rapid Commun.* **2000**, *21*, 117–132.

(3) Tsuji, H.; Ikada, Y. *Polymer* **1995**, *36*, 2709–2716.

(4) Tsuji, H.; Noda, S.; Kimura, T.; Sobue, T.; Arakawa, Y. *Sci. Rep.* **2017**, *7*, 45170.

(5) Eling, B.; Gogolewski, S.; Pennings, A. J. *Polymer* **1982**, *23*, 1587–1593.

(6) Gogolewski, S.; Pennings, A. J. *J. Appl. Polym. Sci.* **1983**, *28*, 1045–1061.

(7) Leenslag, J. W.; Gogolewski, S.; Pennings, A. J. *J. Appl. Polym. Sci.* **1984**, *29*, 2829–2842.

(8) Athanasiou, K. A.; Niederauer, G. G.; Agrawal, C. M. *Biomaterials* **1996**, *17*, 93–102.

(9) Hoffman, A. S. *Adv. Drug Deliv. Rev.* **2012**, *64*, 18–23.

(10) Ikada, Y.; Jamshidi, K.; Tsuji, H.; Hyon, S. H. *Macromolecules* **1987**, *20*, 904–906.

(11) Tsuji, H. *Macromol. Biosci.* **2005**, *5*, 569–597.

(12) Tsuji, H. *Adv. Drug Deliv. Rev.* **2016**, *107*, 97–135.

(13) Okihara, T.; Tsuji, M.; Kawaguchi, A.; Katayama, I.; Tsuji, H.; Hyon, S.; Ikada, Y. *J. Macromol. Sci. Part B Phys.* **1991**, *B30*, 119–140.

(14) Nishino, T.; Matsui, R.; Nakamae, K. *J. Polym. Sci. Part B Polym. Phys.* **1999**, *37*, 1191–1196.

(15) Nakamae, K.; Nishino, T.; Shimizu, Y.; Matsumoto, T. *Polym. J.* **1987**, *19*, 451–459.

(16) Nakamae, K.; Nishino, T.; Ohkubo, H. *J. Macromol. Sci. Part B* **1991**, *30* , 1–23.

(17) Nakamae, K.; Nishino, T.; Ohkubo, H.; Matsuzawa, S.; Yamaura, K. *Polymer*

1992, *33*, 2581–2586.

(18) De Oca, H. M.; Ward, I. M. *J. Polym. Sci. Part B Polym. Phys.* **2007**, *45*, 892–902.

(19) Wasanasuk, K.; Tashiro, K. *Macromolecules* **2012**, *45*, 7019–7026.

(20) Zhang, J.; Duan, Y.; Sato, H.; Tsuji, H.; Noda, I.; Yan, S.; Ozaki, Y. *Macromolecules* **2005**, *38*, 8012–8021.

(21) Sawai, D.; Takahashi, K.; Sasashige, A.; Kanamoto, T.; Hyon, S.-H. *Macromolecules* **2003**, *36* , 3601–3605.

(22) Henton, D. E.; Gruber, P.; Lunt, J.; Randall, J. Chapter 16. Polylactic acid technology. *Nat. Fibers, Biopolym. Biocomposites* **2005**, 527–578.

(23) Fischer, E. W.; Sterzel, H. J.; Wegner, G. *Kolloid-Z. u. Z. Polym.* **1973**, *251*, 980–990.

(24) Tsuji, H.; Ikada, Y.; Horii, F.; Nakagawa, M.; Odani, H.; Kitamaru, R. *Macromolecules* **1992**, *25*, 4114–4118.

(25) Hoogsteen, W.; Postema, A. *Macromolecules* **1990**, *23*, 634–642.

(26) Nakamae, K.; Nishino, T.; Yokoyama, F.; Matsumoto, T. *J. Macromol. Sci. Part B* **1988**, *27*, 407–420.

(27) Inai, R.; Kotaki, M.; Ramakrishna, S. *Nanotechnology* **2005**, *16*, 208–213.

(28) Mezghani, K.; Spruiell, J. E. *J. Polym. Sci. Part B Polym. Phys.* **1998**, *36*, 1005–1012.

(29) Treloar, L. R. G. *Polymer* **1960**, *1*, 279–289.

(30) Treloar, L. R. G. *Polymer* **1959**, *1*, 95–103.

(31) Kobayashi, J.; Asahi, T.; Ichiki, M.; Oikawa, A.; Suzuki, H.; Watanabe, T.; Fukada, E.; Shikinami, Y. *J. Appl. Phys.* **1995**, *77*, 2957–2973.

(32) Nakamae, K.; Nishino, T.; Takagi, S. *J. Macromol. Sci. Part B* **1991**, *30*, 47–62.

(33) Lee, S.; Hongo, C.; Nishino, T. *Macromolecules* **2017**, *50*, 5074–5079.

(34) Ney, J. F. Physical properteis of crystals; Oxford at the Clarendon Press, Oxford, U.K., 1957.

(35) Brizzolara, D.; Cantow, H. J.; Diederichs, K.; Keller, E.; Domb, A. J. *Macromolecules* **1996**, *29*, 191–197.

(36) Zhang, F.; Wang, H. W.; Tominaga, K.; Hayashi, M.; Lee, S.; Nishino, T. E. *J. Phys. Chem. Lett.* **2016**, *7*, 4671–4676.

CHAPTER IV

Structure and Properties of Poly (Decamethylene Terephthalamide)

4.1 Introduction

Recently, polymer materials are used as many industrial field such as automobiles and electronic devices with the advancement of high performance and high functionality. In automobile industry, the weight reduction for fuel efficiency is needed, therefore low weight polymer materials is paid attention. In addition, for alternative of metals and ceramics, it is important to develop high heat resistant polymer materials.

One of alternative oil based polymer, bio based polymers was paid attention to use a material. Poly(decamethylene terephthalamide) (PA10T) is one of bio based polymer. More than 50% of resources are biomass, and PA10T is synthesized from materials derived by inedible castor oil. In addition, PA10T is expected to be used as super engineering plastics due to possess high melting point (315 ° C) and high crystallinity [1-3].

The polymer chains are packed as the most stable state in the crystalline regions according to the chain axis depending on the polymer. For example, depending on the crystal constants (the length (a,b,c) and angle (α, β, γ) of crystals), there show different lattice system. Through these constants factor, it is possible to investigate the exact lattice system, and suggest the exact crystal structure. There are lots of different lattice system, for example, orthorhombic ($a \neq b \neq c$, $\alpha = \beta = \gamma = 90°$), monoclinic ($a \neq b \neq c$, $\alpha = \gamma = 90°$, $\beta \neq 90°$) and triclinic ($a \neq b \neq c$, $\alpha \neq \beta \neq \gamma \neq 90°$) and so on.

As similar chemical structure poly(nonamethylene terephthalamide) (PA9T) was reported such as lattice spacing with 2 molecular as orthorhombic, crystal modulus E_l value as 40 GPa, mechanical properties and thermal properties. However, it is not clear yet about the lattice system of PA10T. Compared with PA9T, PA10T possess one

additional methyl group in main chain, and show difference structure and properties [4]. The reason of difference between PA9T and PA10T could be investigated by analysis of exact structure. Therefore, the lattice system of PA10T was investigated first.

Based on the information of the lattice system of the PA10T, it is possible to measure the crystal modulus in the directions parallel (E_l) to the chain axis by X-ray diffraction [5-6]. The E_l value gives us information about the skeletal conformation, deformation mechanism, and maximum modulus for the specimen modulus of polymers. The E_l values for polymers with fully extended planar zigzag conformation, such as polyethylene (PE) show 235 GPa, whereas *it*.PP (helical structure) show the E_l value as 33 GPa. This low E_l value of *it*.PP is due to helical skeleton, because helical skeleton is easy to elongate to the stress direction compared with the planar zigzag one. About this explanation was detailed at Chapter 1 and 3.

In this chapter, it is investigate the exact lattice constant by X-ray diffraction first, then based on this information, the crystal modulus E_l was measured. In addition, structure and properties in the crystalline regions were investigated. Not only crystal structure and properties, also about the bulk mechanical properties, thermal properties, and surface properties of PA10T were investigated.

4.2. Experimental

4.2.1. Sample preparation

PA10T pellets were kindly supplied from Unitika a Ltd. (Xecot®). PA10T pellets were hot-pressed at 350 ℃, following by 40 ℃ water quenching. Then, PA10T film (film thick

50 μm) was uniaxially drawn 5 times it original length (20 mm) at 180 °C, following by annealing at 230 ℃ for 1h at the constant length. PA10T is generally hard to draw due to its fast crystallization, but we succeeded at attaining a high draw ratio sample just after quenching prior to crystallization starting.

4.2.2. Measurement

Meridional and equatorial X-ray diffraction profiles were carried out by using the Cu$K\alpha$ radiation (λ = 1.54 Å), generated with an RINT-2000 (Rigaku Co.) at 40 kV and 20 mA, as laboratory scale.

Synchrotron X-ray diffraction photograph was measured at SPring-8 BL03XU (R&D beamline). X-Ray wavelength is 0.08266 nm (beam size 0.07 mm (horizontal) x 0.5 mm (vertical)). X-ray fiber photograph of the unloaded PA10T film recorded on a flat-type imaging plate (IP). The sample was exposed to X-ray for 1 s. The sample to detector distance was 224.5 mm.

For crystal modulus, the lattice extension under a constant load was measured by means of an X-ray diffractiometer equipped with a stretching device and a load cell. The strain ε and the stress σ in the crystalline regions, crystal modulus E_l and E_t were measured and calculated with the same method described in Chapter 1.

The tensile properties measurement undrawn and drawn & annealed PA10T films were basically the same with those in Chapter 1. The calculation of the cross-sectional area for PA10T was evaluated from the density, weight, and length of the sample. The means and standard deviations were evaluated for the macroscopic specimen modulus (Y_l), tensile

strength (σ_{max}), and elongation at break (ε_{max}) measured for five samples.

The dynamic viscoelastic properties of PA10T film (20 mm long) were measured the same method with those in Chapter 1.

The melting point (T_m) of PA10T was measured the same method with those in Chapter 1. The sample weight is 5 mg, and a heating rate of 5 ℃/min. T_m was determined as a peak temperature.

To estimate the surface free energy, dynamic contact angles were measured. The dynamic contact angle of water and diiodomethane were measured at room temperature. The advancing contact angle (θ_a) and receding contact angle (θ_r) were measured while the droplet enlarged (< 2mm diameter) and reduced in size, respectively. The surface free energy γ_s of the polymer solid was calculated using the contact angles by Equations. (4.1) and (4.2), which were proposed by Owens and Wendt [7] who extended the Fowkes concept [8].

$$\gamma_s^d + \gamma_s^p = \gamma_s \tag{4.1}$$

$$2\,(\gamma_s^d \gamma_l^d)^{1/2} + 2\,(\gamma_s^p \gamma_l^p)^{1/2} = (1 + \cos\theta)\gamma_l \tag{4.2}$$

where γ_l is the surface free energy of the liquid, and γ_s^d and γ_s^p are its dispersion and polar components, respectively. The γ_l^d and γ_l^p values of water are 21.8 and 51.0 mJ/m^2 and those of diiodomethane are 48.5 and 2.3 mJ/m^2, respectively [7] . And, an average of 15 readings was used for the contact angle determination.

4.3. Results and Discussion

4.3.1. Crystal lattice

Figure 4.1 show meridional X-ray diffraction profile and the angle φ of inclination for the (002) plane of PA10T film along the Debye-Scherrer ring, together with expansion of profile. Around 2θ = 4.5 °, one strong and shape peak was observed. By Bragg's equation, that peak's lattice spacing was calculated as 19.6 Å . In fact, the c axis length for the fully extended planar zigzag skeleton of PA10T was evaluated by using reported bond lengths, bond angles and these force constants, as 21.6 Å , which is similar value compared with observed value. As mentioned in introduction, PA9T is composed 2 molecular in the crystal. Assuming PA10T is also composed 2 molecular for c axis lattice constant, the 2θ = 4.5 ° peak is suggest to 002 reflection. Then, 2θ = 13.2 °, 22.3 °, 26.4 °, 30.5 °, 40.5 °,

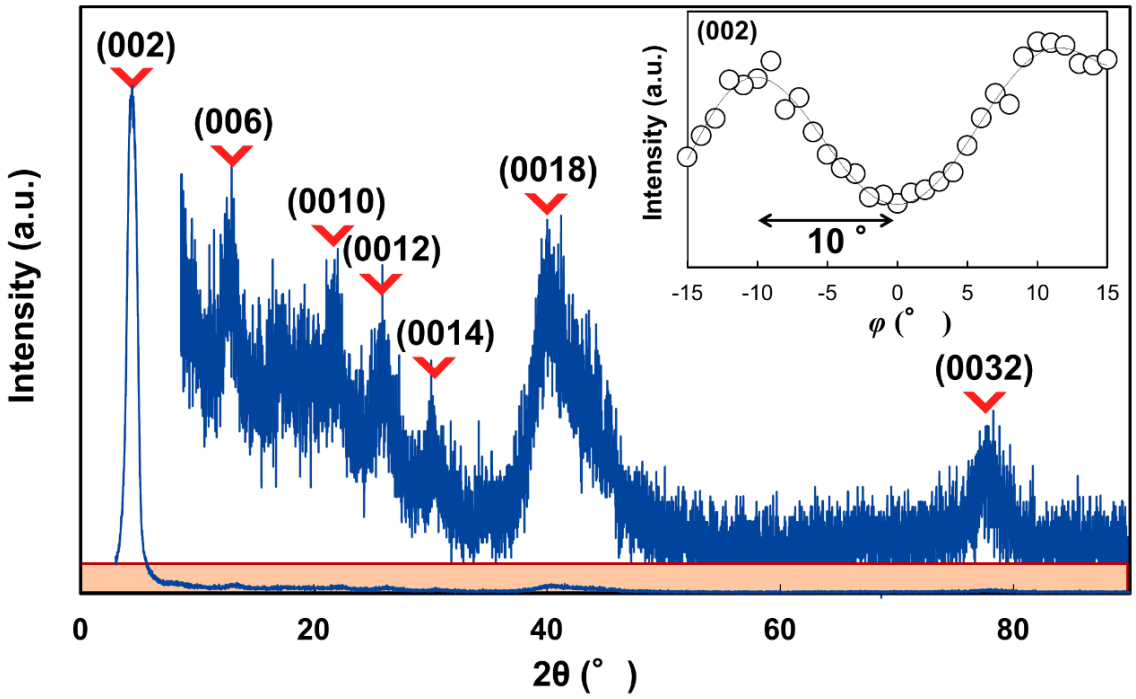

Fig. 4.1 Meridional X-ray diffraction profile and the angle φ of inclination for the (002) plane of PA10T film along the Debye-Scherrer ring.

77.9 ° could be calculated the lattice spacing and lattice plane, then there were 006, 0010, 0012, 0014, 0018, 0032 reflections, show in figure 4.1, respectively. Concerning these values, the average lattice spacing of all reflections was 40.1 Å as PA10T c axis length.

In addition, angle φ of inclination for the (002) plane of PA10T film along the Debye-Scherrer ring show in figure 4.1. The (002) plane was inclined for 10 ° from c axis, the (0032) plane was also prove as 10 ° of inclination (not shown in this thesis). This suggest PA10T possesses as lattice constant angle α and γ is 90 °, but β is inclined as 80 °.

Figure 4.2 show equatorial X-ray diffraction profile of PA10T film. From X-ray diffraction profile, 2θ = 21.3 ° (strong), 27.5 °, 36.4 ° (small) was observed. There were 4.17, 3.24, 2.47 Å as lattice spacing by Bragg's equation. The concept of reciprocal lattice spacing for normalize the lattice spacing (by reciprocal of the values) was adopted. When

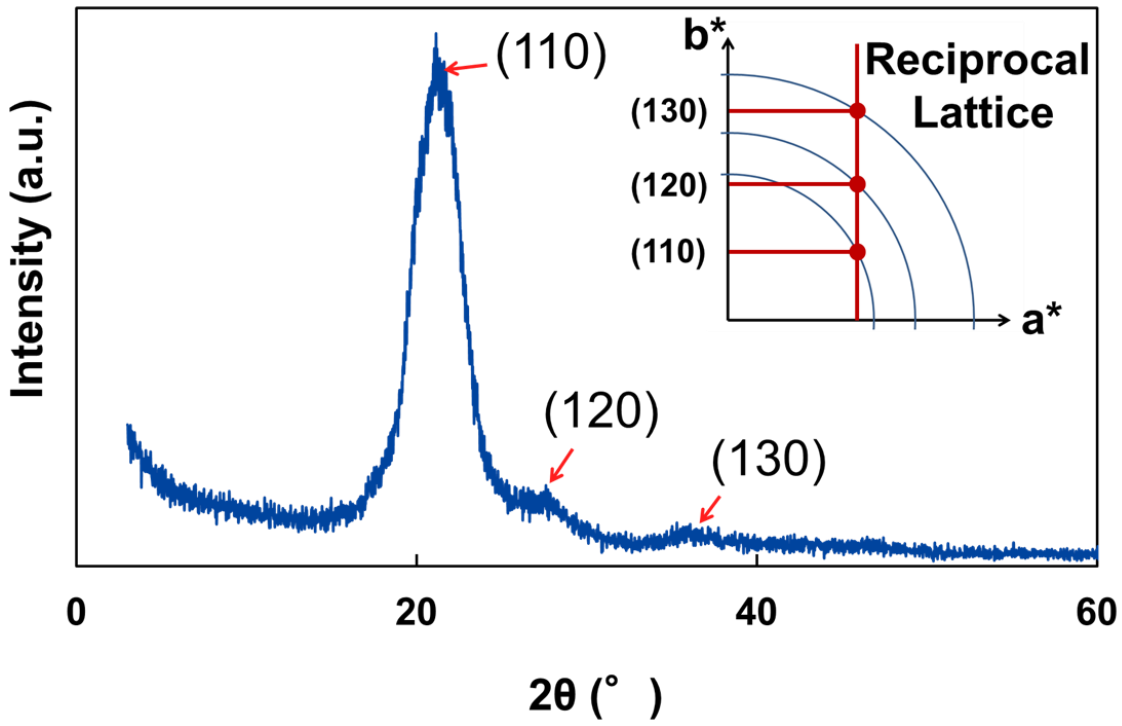

Fig. 4.2 Equatorial X-ray diffraction profile of PA10T film

α, γ = 90 ° in *ab* plane, the reciprocal lattice spacing could show as in figure 4.2. In reciprocal lattice model, there were determined as 110, 120 and 130, respectively. Here, the *a* and *b* axis were calculated as *a* = 4.8 Å and *b* = 8.7 Å . Compared with the *a* and *b* length of PA9T (a = 4.96 Å and b = 8.39 Å) [9], that of PA10T show similar value.

Compared with PA9T, PA10T is composed one more methyl group in molecular chain. Even, *c* axis lattice constant was different, but the *a* and *b* axis length was maintained, which trend is similar to other polymers. The unit cell system of PA10T is monoclinic in the crystalline regions.

Figure 4.3 show X-ray fiber photograph of PA10T film, measured at SPring-8, BL03XU. For meridional direction, there are many split reflections. It suggest PA10T possess

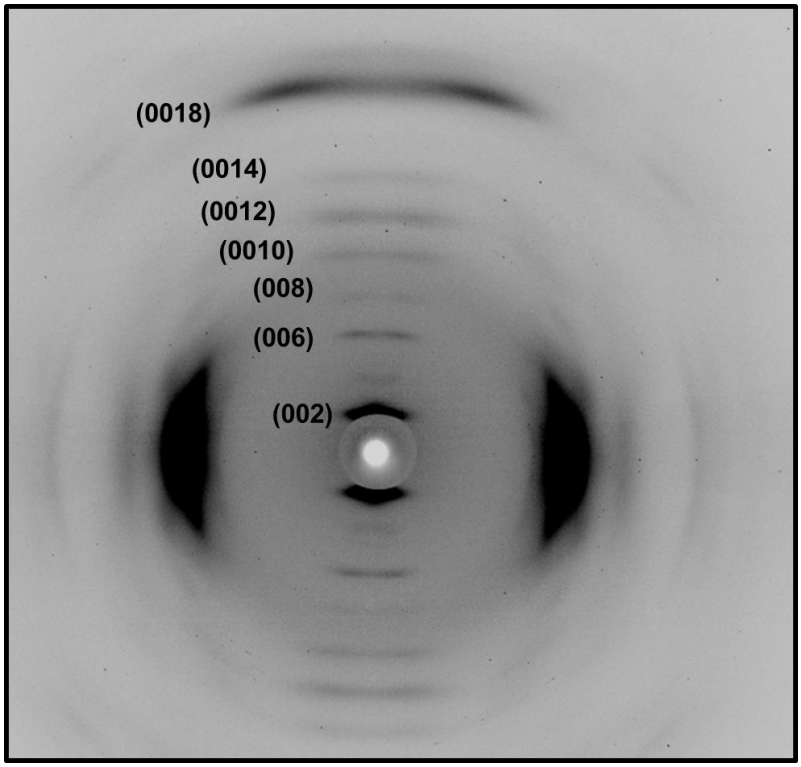

Fig. 4.3 X-ray fiber photograph of PA10T film (SPring-8, BL03XU).

helical structure in the crystal regions. For equatorial direction, one strong reflection showed asymmetric shape, suggest to overlap with many reflections.

With above results, comparing with the c axis length assuming fully extended planar zigzag conformation of PA10T as 43.3 Å , but the observed value of PA10T is 40.6 Å , as approximately 6.5 % contraction from planar zigzag conformation. This is suggested that helical structure in the crystalline regions caused the largely contraction of PA10T. Based on these lattice constant information of PA10T, then the mechanical properties in the crystalline regions were investigated below.

4.3.2. Crystal properties

Figure 4.4 shows the stress σ - strain ε curves for the (0032) plane of PA10T at 300 K. In fact, the (006), (0010), (0012), (0014) plane is not proper to measure the crystal modulus due to overlapping of peaks very much. About the (0018) plane, the peak shape is obviously asymmetric, indicate to possess multiple reflections and not proper to measure the crystal modulus. Due to these reasons, only the (0032) plane was adopted for crystal modulus measurement. All the plots could be expressed with the straight line with the same inclination through the origin, and the lattice extensions were always reversible. The inclination of this line gave the crystal modulus E_l of PA10T as 26 GPa at 300 K. The E_l of PA10T is much lower than that (235 GPa) of polyethylene (PE) or (260 GPa) of poly(vinyl alcohol) (PVA) with fully extended planar zigzag conformation in the crystalline regions. As mentioned above, the PA10T skeleton is contracted, and possess helical conformation in the crystalline regions. It is considered that contracted helical

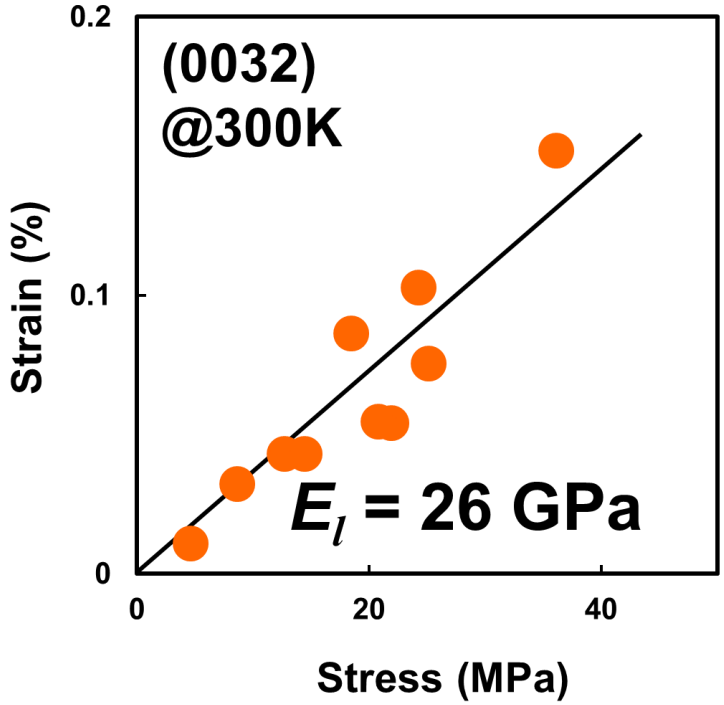

Fig. 4.4 Stress-strain curves for the (0032) plane of PA10T at 300K.

skeleton bring low E_l value of PA10T. Tashiro *et al*. calculated E_l value of PA10T as 64 GPa, however, the observed E_l value of PA10T show lower value than that of calculated value. This is because, PA10T is already largely contracted in the crystalline regions [10].

Figure 4.5 show the relationship between the crystal modulus E_l and the chain contraction of the planar zigzag conformation of PA10T and various polymers to compare, measured by Nishino Laboratory so far. The crystal modulus E_l decreases for all series of polymers of poly(α-olefin), polyesters, polyamide as the chain contraction increases. (The decreasing trend could express as blue shadow and more examples showed in Nishino Laboratory publications). Only few percent of contraction, polymers especially the series of nylons manifest lower E_l values. Tashiro *et al*. calculated the trend of crystal modulus for the series of nylons, as dotted red line in figure 4.5 [11]. The observed crystal modulus trend coincide to the calculation of crystal modulus.

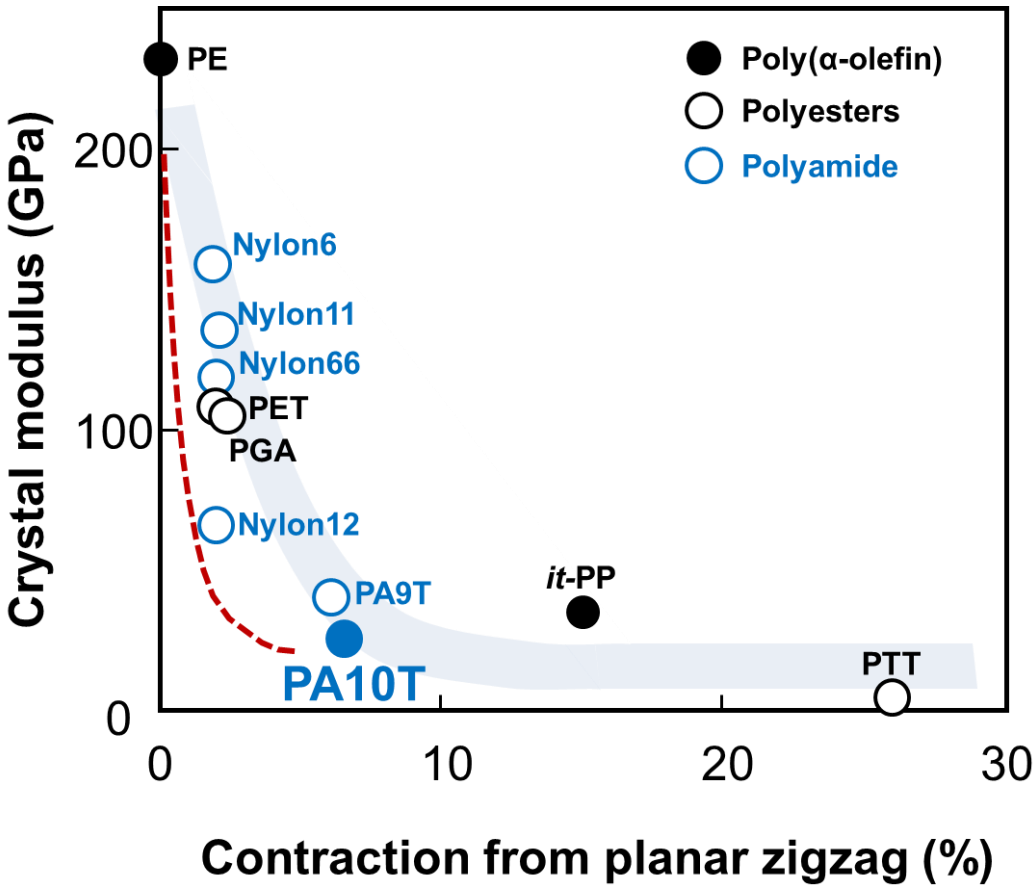

Fig. 4.5 Relationship between the crystal modulus E_l and the chain contraction from the planar zigzag conformation of various polymers with PA10T.

Table 4.1 The E_l value, cross-sectional area (S), f –values and chain contraction in the crystalline regions of PA10T and various polymers.

	E_l	S	f–value	Contraction
	GPa	nm^2	10^{-10} N	%
PE	235	0.182	4.28	0
PGA	104	0.162	1.68	2.4
PA9T	40	0.208	0.83	5.9
PA10T	26	0.209	0.54	6.5

Table 4.1 show the E_l value, cross-sectional area (S), *f* -values and chain contraction in the crystalline regions of PA10T and various polymers. The *f* -values means the force required to stretch a molecule by 1%. And, the *f* -values were corrected by cross-sectional area, then *f*-value could be compared the polymer molecular chain rigidity, directly. Significantly, increasing of contraction from planar zigzag conformation in the crystalline, E_l value and *f*-value decrease for all polymers. These low E_l value and *f*-value of PA10T suggest that PA10T can be used as a flexible material. Compare with PA9T, PA10T show even lower E_l value with higher contraction. The existence/ absence of one methyl groups inserted on the main chain, the results of PA10T and PA9T show quite different.

4.3.3. Bulk properties

Table 4.2 show exact specimen modulus (Y_l), tensile strength (σ_{max}), elongation at break (ε_{max}), stiffness (K), glass transition temperature (T_g) and melting temperature (T_g) of undrawn and drawn & annealed PA10T films. Figure 4.6 show stress-strain curves of undrawn and drawn & annealed PA10T films. Undrawn PA10T show low Y_l and σ_{max} ,

Table 4.2 Specimen modulus (Y_l), tensile strength (σ_{max}), elongation at break (ε_{max}), stiffness (K), glass transition temperature (T_g) and melting temperature (T_m) of undrawn and drawn & annealed PA10T films.

PA10T	Y_l (GPa)	σ_{max} (MPa)	ε_{max} (%)	K (J/g)	T_g (°C)	T_m (°C)
Undrawn film	1.5	110	247	110	115	309
Drawn & annealed film	5.4	510	12	22	139	310

whereas ε_{max} and K show high value compared with other polymers. These suggest PA10T is proper to be used as a flexible material, which need high toughness. Or, after drawn and annealed process, mechanical properties (Y_l and σ_{max}) of PA10T show higher than that of undrawn PA10T. Therefore, PA10T is possible to control the properties for the needs.

Figure 4.7 show temperature dependence of the storage modulus (E'), loss modulus (E'') and tan δ of PA10T film. The storage and loss modulus were maintained high value for all temperature. These high storage and loss modulus of PA10T suggest that PA10T is very stable against the heat. In addition, there were two peak around 210 K and 410 K for tan δ. The higher peak could be alpha (α) transition temperature, as glass transition

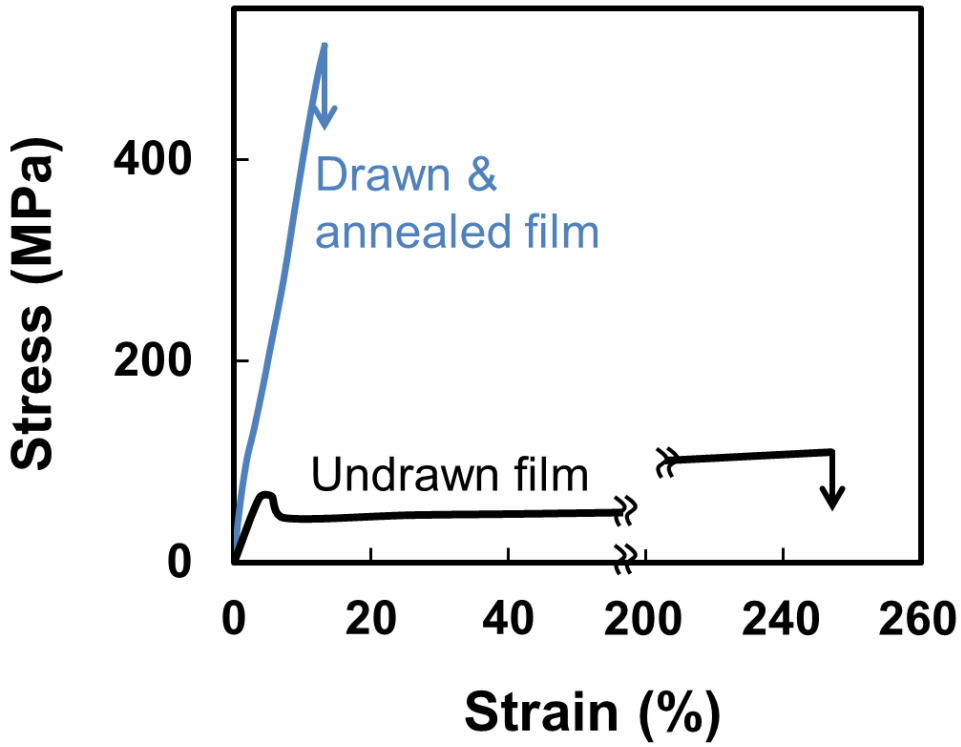

Fig. 4.6 Stress-strain curves of undrawn and drawn & annealed PA10T films.

temperature (T_g, exact value show in Table 2).Then the lower peak could be beta (β) transition. (About α and β transition was detailed at Chapter 1.)

From the results of DSC measurement, the melting temperature (T_m) of PA10T show ~310 ℃ (Table 4.2). Even drawing process, T_m values were not changed. As a result, this higher melting temperature, maintaining high storage and loss modulus at high temperature strongly support to be qualified for the super engineering plastic.

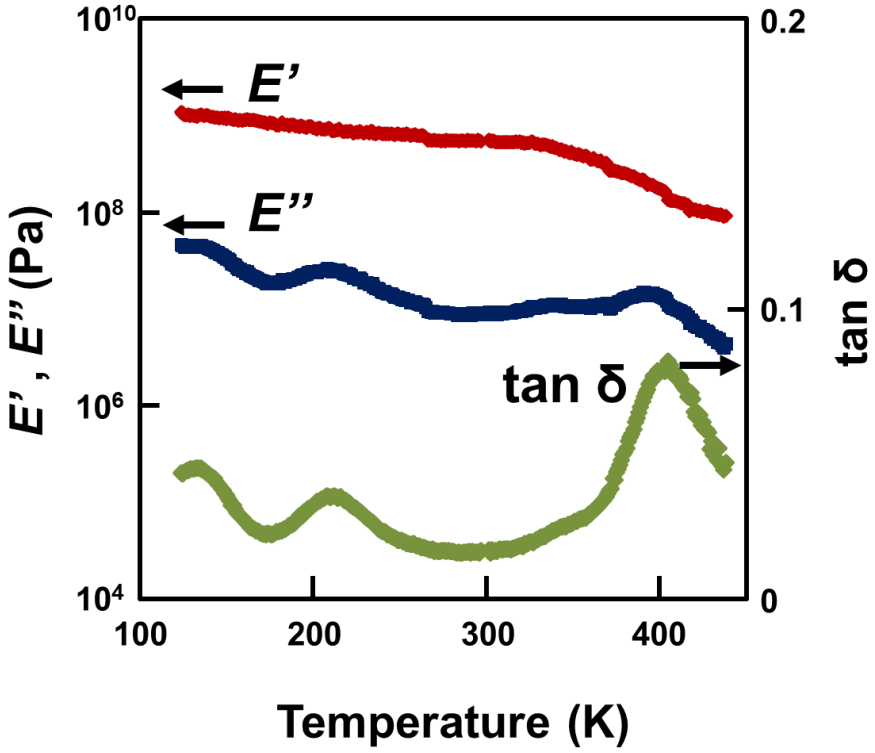

Fig. 4.7 Temperature dependence of the storage modulus (*E'*), loss modulus (*E''*) and tan δ of PA10T film.

4.3.4. Surface properties

Table 4.3 show surface free energy γ, γ^d and γ^p are its dispersion and polar components of PA10T. The surface free energy of PA10T is 46.3 mJ/m^2, when 29.1 mJ/m^2 and 47.5 mJ/m^2 for *it*.PP and nylon6, respectively. For example, the γ value of other polymers show as polyethylene (36 mJ/m^2) and polytetrafluoroethylene (PTFE) (22 mJ/m^2) [12]. The γ value of PA10T is higher than that of *it*.PP and PTFE, but similar to that of nylon6. This suggest that the PA10T possess higher wettability (hydrophilic) than *it*.PP but as same as nylon 6. Noteworthy, PA10T and nylon6 show much higher γ^p values than that of *it*.PP. These suggest that *it*.PP only based on van der Waals interaction in the molecular, therefore dispersion interaction superior to polar interaction, when PA10T and nylon possess higher polar interaction due to the functional group in molecular.

Table 4.3 Contact angle θ and surface free energy γ of PA10T, Nylon6, Nylon66, *it*.PP.

Polymers	Water				Methylene iodide				Surface free energy		
	θ_a	θ_r	θ	Δ	θ_a	θ_r	θ	Δ	γ	γ^d	γ^p
	degree				degree				mJ/m^2		
PA10T	78	39	60	39	47	31	40	16	46.3	31.5	14.8
Nylon 6	77	45	62	32	45	27	37	18	47.5	32.6	14.9
Nylon 66	86	48	68	38	49	38	44	9	42.9	30.3	12.6
it.PP	105	99	95	16	65	59	54	6	29.1	28.5	0.56

4.4. Conclusions

From meridional X-ray diffraction with the angle φ of inclination of PA10T, the lattice constant of *c* axis lattice constant as 40.1 Å, and angle of β is inclined as 80 ° in the crystalline regions. In addition, from equatorial X-ray diffraction of PA10T film, the *a* and *b* axis were calculated as *a* = 4.8 Å and *b* = 8.7 Å. Compared with the a and b axis of PA9T (a = 4.96 Å and b = 8.39 Å), that of PA10T show similar value. As a result, the unit cell system of PA10T suggest to possess the monoclinic in the crystalline regions. From the X-ray fiber photograph, PA10T consider to possess helical structure in the crystal regions. By crystal modulus $E_{l,}$ PA10T show 26 GPa at 300 K. The E_l of PA10T is much lower than that PE, due to helical structure in the crystalline regions. Because PA10T contracted largely, PA10T show lower E_l value than that of PA9T. About the mechanical properties, PA10T is proper to be used as a flexible material because PA10T show high toughness than other polymers. Or, with drawing and annealing process, PA10T is possible to control the properties for the needs. In addition, the high melting temperature, maintaining high storage and loss modulus at high temperature strongly support to be qualified for the super engineering plastic. Moreover, the γ value of PA10T is higher than that of *it*.PP, and similar to that of nylon6. This suggest that the PA10T possess higher wettability (hydrophilic) than *it*.PP but as same as nylon 6.

4.5. References

(1) Novitsky, T. F.; Lange, C. A.; Mathias, L. J.; Osborn, S.; Ayotte, R.; Manning, S. *Polymer* **2010**, *51* (11), 2417–2425

(2) Li, M.; Dingemans, T. J. *Polymer* **2017**, *108*, 372–382

(3) Li, M.; Bijleveld, J.; Dingemans, T. J. *Eur. Polym. J.* **2018**, *98*, 273–284

(4) Yamamoto, H.; Tashiro, K.; Ishino, K.; Takahashi, M.; Endo, R.; Asada, M.; Li, Y.; Katsube, K.; Ishii, T. *Polymer* **2017**, *116*, 378–394

(5) Lee, S.; Hongo, C.; Nishino, T. *Macromolecules* **2017**, *50* (13), 5074–5079

(6) Nishino, T.; Okamoto, T.; Sakurai, H. *Macromolecules* **2011**, *44* (7), 2106–2111

(7) Owens, D. K.; Wendt, R. C. *J. Appl. Polym. Sci.* **1969**, *13* (8), 1741–1747

(8) Fowkes, F. M. *J. Phys. Chem.* **1963**, *67* (12), 2538–2541

(9) Uddin, A. J.; Gotoh, Y.; Ohkoshi, Y.; Nishino, T.; Endo, R. *Polym. Eng. Sci.* **2012**, *52* (2), 331–337

(10) Yamamoto, H.; Tashiro, K.; Asada, M.; Katsube, K. *Polym. Prepr. Jpn.*, **2015**, *64* (2), 1F08

(11) Tashiro, K.; Tadokoro, H. *Macromolecules* **1981**, *14*, 781–785

(12) Sumiya, K.; Taii, T.; Nakamae, K.; Matsumoto, T. J. *Adhes. Soc. Jpn.*, **1982**, *18*, 345.

CONCLUSIONS

In this thesis, structure and properties of bio based polymers were investigated.

To prevent environmental damage by mass-produced plastic products, biodegradable bio based polymers are expected to be used as next generation disposable materials as alternative oil based polymer. Bio based polymers are synthesized by biomass such as tree, grain, and grass. Bio based polymers are paid attention materials as eco friendly without exhaustion. In addition, biodegradable bio based polymers could be permanent recyclable, and will be good way to conserve the energy. Among biodegradable bio based polymers, poly(glycolic acid)(PGA), poly(lactic acid) (PLA) and poly(decamethylene terephthalamide) (PA10T) were adopted.

For using polymers, it is necessary to control the polymer properties such as mechanical, thermal properties or surface interface for the needs. Among polymer structure, crystalline regions are most important factor. These crystalline regions contribute to the polymer properties directly. Therefore, it is most important to investigate the exact crystal structure and properties. In this thesis, the crystal modulus was used for investigating the crystal properties. For example, crystal modulus in the direction parallel (E_l) and perpendicular (E_t) to the chain axis give information about skeletal conformation, deformation mechanism, maximum modulus and intermolecular interaction, anisotropies of polymers, respectively. Also, in order to exclude the thermal factor in the polymers, crystal modulus was measured at cryogenic temperature, and investigated the temperature dependence of polymers from cryogenic temperature to high temperature.

In **Chapter 1**, crystal modulus of PGA was investigated. PGA was used only limited fields such as sutures, but has succeeded in mass-producing, recently. However, there are not studied about mechanical properties and thermal properties. Especially, about high

melting point of PGA was not clarified the reason compared with other aliphatic polyesters. Therefore, mechanical properties and thermal properties were investigated by crystal modulus. Crystal modulus in the directions parallel (E_l) and perpendicular (E_t) to the chain axis of poly(glycolic aicd) (PGA) were measured by X-ray diffraction. The crystal modulus E_l of PGA shows low value (104 GPa) compared with that of polyethylene (235 GPa) or calculated value (237 GPa) which assumed fully extended planar zigzag conformation in the crystalline regions. This suggest that a PGA skeleton is not fully extended but contracted from a planar zigzag one, through the internal rotation. The E_l value of PGA shows temperature dependence from cryogenic temperature to high temperature. Even at cryogenic temperature, PGA chain did not reach a fully extended state but contracted. This suggests the PGA skeleton is intrinsically contracted in the crystalline regions. Also around 200 K, abrupt changes of both E_l values and chain contraction were considered to be caused by molecular motion in the crystalline regions. On the other hands, the high crystal modulus E_t of PGA suggested high intermolecular interaction acts between PGA chains. Both the low E_l value and high E_t value are considered to contribute to the high melting point of PGA. Considering above results, the crystal structure and properties, especially, the reason of high melting point of PGA became clear.

In **Chapter 2**, highly aligned, oriented, crystallized PGA nanofibers were prepared by electrospinning methods, and investigated the properties. Based on the information of crystal properties at Chapter1 (especially, maximum modulus was known by crystal modulus), PGA nanofibers were prepared and compared the properties in order to achieve the maximum modulus. PGA nanofiber was electrospun with the use of rotating drum collector to align nanofibers. Aligned nanofibers could be drawn 4 times, then annealed.

The drawn and annealed PGA nanofibers showed not only high orientation (X-ray fiber photograph), but also high mechanical properties (tensile test) compared with those of cast film. As a results, drawn & annealed nanofibers show high Young's modulus (6.8 GPa), tensile strength (201 MPa). Both the crystallite orientation and mechanical properties were found to be increased by drawing & annealing of PGA nanofibers. Though, the mechanical properties of PGA nanofibers could not reach to maximum modulus, only as 7 %, however, this Young's modulus resemble that of electrospun/ drawn *it*.PP nanofibers. Therefore, PGA nanofibers are expected to be used as an alternative material in many fields which requires the same modulus of *it*.PP.

In **Chapter 3**, crystal modulus of PLA was investigated. The crystal modulus of poly(L-lactic acid) (PLLA) was evaluated experimentally and theoretically, but only the crystal modulus of PLLA along the chain direction at room temperature is insufficient for overviewing the relationship between structure and properties of a series of PLA. In addition, there are no reasonable explanation on the melting point of scPLA is more than 50 degree higher than those of PLLA and PDLA. The crystal modulus of not only PLLA, but also those of PDLA and scPLA, including their crystal moduli both in the directions parallel and perpendicular to the chain axis were investigated. In addition, temperature dependence of the crystal modulus of PLLA, PDLA, and scPLA were also investigated in this Chapter to examine the thermal properties of the crystalline regions of PLAs. PLLA and PDLA possesses same E_l value as 14 GPa, even though, they possess opposite chain helical direction, at room temperature. This small E_l value is caused by largely contracted 10_3 helical structure in the crystalline regions for PLLA and PDLA. The E_l value of scPLA is 20 GPa at room temperature, being higher than those of PLLA and PDLA. This is due to that the skeleton of scPLA is slightly extended (3_1 helix) than those of PLLA and PDLA.

All PLLA, PDLA and scPLA showed temperature independence of the E_l values from cryogenic temperature to room temperature, which is considered that the structural effect on the E_l value is higher than the temperature effect. Even with the existence/ absence of methyl groups inserted on the side chain, the results of PLA was quite different from those of PGA 25. The E_t values of PLLA and PDLA were smaller than that of PE. These suggest that only weak van der Waals intermolecular interactions act in PLLA and PDLA. The E_t value of scPLA was slightly higher than those of PE, PLLA and PDLA, however, they was lower than that based on hydrogen bonding. However, this slightly higher E_t value of scPLA contribute to possess higher melting point compared with those of PLLA and PDLA.

In **Chapter 4**, the crystal structure and properties of PA10T. From meridional X-ray diffraction with the angle φ of inclination of PA10T, the lattice constant of c axis length as 40.1 Å , and angle of β is inclined as 80 ° in the crystalline regions. In addition, from equatorial X-ray diffraction of PA10T film, the *a* and *b* axis were calculated as *a* = 4.8 Å and *b* = 8.7 Å . Compared with the a and b axis of PA9T (a = 4.96 Å and b = 8.39 Å), that of PA10T show similar value. Therefore, the unit cell system of PA10T is monoclinic in the crystalline regions. From the X-ray fiber photograph, PA10T consider to possess helical structure in the crystal regions. From crystal modulus E_l, PA10T show 26 GPa at 300 K. The E_l of PA10T is much lower than that PE, due to helical structure in the crystalline regions. About the mechanical properties, PA10T is proper to be used as a flexible material because PA10T show high toughness than other polymers. In addition, the high melting temperature, maintaining high storage and loss modulus at high temperature strongly support to be qualified for the super engineering plastic.

In summary, the relationship between structure and properties of bio based polymers PGA, PLA and PA10T were described, with application of PGA as a nanofibers. Based on the information of this thesis, the development as practical materials could be expected.

List of Achievements

Publications

Chapter 1

1. Crystal Modulus of Poly (glycolic acid) and Its Temperature Dependence

Sunglin Lee, Cizuru Hongo, Takashi Nishino

Macromolecules **2017**, *50*, 5074-5079.

Chapter 3

2. Crystal modulus of Poly (lactic acid)s, and their Stereocomplex

Sunglin Lee, Masayuki Kimoto, Masakazu Tanaka, Hideto Tsuji, Takashi Nishino *Polymer*, accepted in 18th of Jan. 2018.

The author also contributed to the following paper.

3. Elucidation of Chiral Symmetry Breaking in a Racemic Polymer System with Terahertz Vibrational Spectroscopy and Crystal Orbital Density Functional Theory

Feng Zhang, Houng-Wei Wang, Keisuke Tominaga, Michitoshi Hayashi, Sunglin Lee, Takashi Nishino

J.Phys.Chem.Lett, **7**, 4671–4676, 2016

4. ポリグリコール酸の結晶弾性率

西野　孝, Sunglin Lee, 本郷　千鶴

ポバール会記録, **第150回**, 1-8, 2017

5. From Korea to Japan, and United Kingdom

Sunglin Lee

繊維学会誌, **73**, 6–7, 2017

Presentations

1. ポリグリコール酸の高融点と結晶弾性率

イ ソンリン，本郷千鶴，小寺賢，西野孝

ポスター，第63回高分子討論会，長崎，2014

2. Elastic Modulus of the Crystalline Regions of Poly(glycolic acid)

Sunglin LEE，Chizuru HONGO，Takashi NISHINO

Oral，第64回高分子学会年次大会 ，札幌，2015

3. Temperature dependence of elastic modulus of the crystalline regions and high melting point of poly(glycolic acid)

Sunglin LEE，Chizuru HONGO，Takashi NISHINO

Oral，The 5th International Conference on Bio-based Polymers (ICBP2015)，Singapore，2015

4. バイオベースポリエステルの結晶弾性率の温度依存性

イソンリン，木本真之，田中正和，本郷千鶴，西野孝

口頭，第64回高分子討論会，仙台，2015

5. Cryogenic Mechanical properties of biobased polyesters

Sunglin LEE，Chizuru HONGO，Takashi NISHINO

Poster, International Symposium on Rheology, (ISR2015), 神戸, 2015

6. Elastic modulus of the crystalline regions of biobased polyesters

Sunglin LEE, Chizuru HONGO, Takashi NISHINO

Oral, The 2015 International Chemical Congress of Pacific Basin Societies (PACIFICHEM 2015), Hawaii, 2015

7. ポリデカメチレンテレフタルアミドの結晶構造と力学物性

イ ソンリン, 三井淳一, 川原光博, 上田一恵, 西野孝

ポスター, 第65回高分子学会年次大会, 神戸, 2016

8. 生分解性高分子の結晶構造と力学物性

Lee Sunglin, 本郷千鶴, 西野孝

ポスター, 第5回 JACI/GSCシンポジウム, 神戸, 2016

9. Structure and properties of electrospun poly glycolic acid nanofiber

Sunglin LEE, Chizuru HONGO, Takashi NISHINO

Poster, 3rd International conference on Bio-based Polymers and Composites (BiPoCo2016), Szeged (Hungary), 2016

10. Mechanical properties of well-alligned and well-oriented poly glycolic acid nanofibers by electrospinning

Sunglin LEE, Chizuru HONGO, Takashi NISHINO

Poster，9th International Conference on Green Composites (ICGC-9)，神戸，2016

11. Elastic modulus of the crystalline regions of poly lactic acid

Sunglin LEE，Chizuru HONGO，Takashi NISHINO

Oral，9th International Conference on Green Composites (ICGC-9)，神戸，2016

12. 耐熱性ポリアミドの結晶構造と力学物性

イ ソンリン，三井淳一，川原光博，上田一恵，西野孝

ポスター， 第6回CSJ化学フェスタ2016，2016

13. 高配向ポリグリコール酸ファイバーの創製と力学物性

イ ソンリン, TU Wei, PEIJS Ton，西野孝

ポスター， 第66回高分子学会年次大会，千葉，2017

14. エレクトロスピニング法を用いた高配列・高配向ポリグリコール酸ナノファイバーの創製と力学物性

イ ソンリン，本郷千鶴，西野孝

口頭，平成29年度繊維学会年次大会，東京，2017

15. Crystal structure and mechanical properties of poly (glycolic acid)

Sunglin LEE，Takashi NISHINO

Poster，8th International Conference on Green and Sustainable Chemistry (GSC8)，メルボルン（オーストラリア），2017

Awards

1. 2015 年 9 月 International Symposium on Rheology, (ISR2015), 神戸, ポスター発表

Best Poster Award 受賞

2. 2016 年 11 月 9th International Conference on Green Composites (ICGC-9), 神戸, ポスター発表,

Best Poster Award 受賞

3. 2016 年 12 月 For Exceptional academic attainment in the Premium Program, KOBE UNIVERSITY

OUTSTANDING STUDENT AWARD 受賞

Acknowledgements

First of all, I would like to express my deepest gratitude to Professor Dr. Takashi Nishino of Department of Chemical Science and Engineering, Faculty of Engineering in Kobe University, for his continuous encouragement, precious suggestions, helpful discussions and advice through my research life. It would have not been possible to continue my experiment and research without his endless patient, deeply expertise guidance and encouragement.

We would like to thank Professor Dr. Shinji Ishida also Professor Dr. Chiaki Ogino of Department of Chemical Science and Engineering, Faculty of Engineering in Kobe University for reviewing the thesis and for their precious advices in public hearing..

I am also thanks to Assistant professor Dr. Chizuru Hongo Organization of Advanced Science and Technology in Kobe University, for her helpful guidance and fruitful suggestions.

I would like to thanks to Associate professor Dr. Takuya Matsumoto of Department of Chemical Science and Engineering, Faculty of Engineering in Kobe University.

All former and present colleagues in Nishino laboratory at Department of Chemical Science and Engineering, Faculty of Engineering in Kobe University are thankfully acknowledged for the great support. I could not continue my research life without their wonderful collaborative effort, useful discussion, and unending encouragement. Dr. Seira Morimune, Dr. Koji Nobuta, Dr. Kaya Tokuda, Mr. Yoshihito Tanaka, Mr. Naoyuki Miki, Mr. Yuji Asahina, Ms. Sae Fujiura, Ms. Eri Morio, Ms. Keiko Mizoguchi, Mr. Keishiro Nishi, Mr. Shintaro Oku, Mr. Tomoki Yudate, Mr. Takashi Kato, Mr. Yuta Nakanishi, Mr. Takuya Ohashi, Mr. Shota Okamoto, Mr. Yosuke Shimizu are specially thank for their wonderful group organizing efforts. The comfortable workplace was absolutely essential for finishing this thesis. They were friendly, kind and cheerful about everything. It was a great honor to be able to work at such a fulfilling group.

I am thanks to all the staffs of Japanese Government (Monbukagakusho: MEXT) Scholarship to give a chance to study in Japan, and support me for 1 year as research student, and 2 year as master student in Kobe University.

Also, I am very thanks to all the staffs of Rotary Yoneyama Memorial Foundation to support me for 2 year at doctoral student in Kobe University.

I am special thanks to all the staffs in the Department of Chemical Science and Engineering, Faculty of Engineering in Kobe University, to give the change to go abroad and research with premium program at Queen Mary College, University of London (QMUL).

And I am thanks to Professor Dr. Ton Peijs to accept to be in a short student at QMUL and advice a lot about the researches. Also thanks to Mr. Wei Tu and Han Zhang for everything owing in QMUL.

I am grateful to all the staffs in the Department of Chemical Science and Engineering, Faculty of Engineering in Kobe University for their support.

I also would like to express my gratitude to Ms. Yoshimi Ozaki in Nishino laboratory at Department of Chemical Science and Engineering, Faculty of Engineering in Kobe University for her invaluable help and encouragement. KTC are acknowledged for the generous financial support.

마지막으로, 박사를 끝낼 때까지 물심양면으로 응원해준 우리 가족 이종호 사장님, 정경애 여사님, 이승하 동생님, 또한 김민지님, 김기현님, 강병준님, 그리고 선생님들 나의 언니들, 오빠들, 친구들, 후배들, 진심으로 감사 드립니다. 받은 은혜 갚으면서 살겠습니다. 감사합니다.

January, 2018

Lee Sung Lin, 이성린

Doctor Thesis, Kobe University
"Structure and Properties of Bio based Polymers", 120 pages
Submitted on January, 19, 2018
The date of publication is printed in cover of repository version published in Kobe University Repository Kernel.

© LEE SUNG LIN
All Right Reserved, 2018